OPEN ACCESS

African Journal of Environmental Science and Technology

November 2023
ISSN 1996-0786
DOI: 10.5897/AJEST
www.academicjournals.org

ACADEMIC JOURNALS
expand your knowledge

About AJEST

African Journal of Environmental Science and Technology (AJEST) provides rapid publication (monthly) of articles in all areas of the subject such as Biocidal activity of selected plant powders, evaluation of biomass gasifier, green energy, Food technology etc. The Journal welcomes the submission of manuscripts that meet the general criteria of significance and scientific excellence. Papers will be published shortly after acceptance. All articles are peer-reviewed

Indexing

The African Journal of Environmental Science and Technology is indexed in:
CAB Abstracts, CABI's Global Health Database, Chemical Abstracts (CAS Source Index), China National Knowledge Infrastructure (CNKI), Dimensions Database, Google Scholar, Matrix of Information for The Analysis of Journals (MIAR), Microsoft Academic

AJEST has an h5-index of 14 on Google Scholar Metrics

Open Access Policy

Open Access is a publication model that enables the dissemination of research articles to the global community without restriction through the internet. All articles published under open access can be accessed by anyone with internet connection.

The African Journal of Environmental Science and Technology is an Open Access journal. Abstracts and full texts of all articles published in this journal are freely accessible to everyone immediately after publication without any form of restriction.

Article License

All articles published by African Journal of Environmental Science and Technology are licensed under the Creative Commons Attribution 4.0 International License. This permits anyone to copy, redistribute, remix, transmit and adapt the work provided the original work and source is appropriately cited. Citation should include the article DOI. The article license is displayed on the abstract page the following statement:

This article is published under the terms of the Creative Commons Attribution License 4.0
Please refer to https://creativecommons.org/licenses/by/4.0/legalcode for details about Creative Commons Attribution License 4.0

Article Copyright

When an article is published by in the African Journal of Environmental Science and Technology, the author(s) of the article retain the copyright of article. Author(s) may republish the article as part of a book or other materials. When reusing a published article, author(s) should; Cite the original source of the publication when reusing the article. i.e. cite that the article was originally published in the African Journal of Environmental Science and Technology. Include the article DOI Accept that the article remains published by the African Journal of Environmental Science and Technology (except in occasion of a retraction of the article) The article is licensed under the Creative Commons Attribution 4.0 International License.

A copyright statement is stated in the abstract page of each article. The following statement is an example of a copyright statement on an abstract page.

Copyright ©2016 Author(s) retains the copyright of this article.

Self-Archiving Policy

The African Journal of Environmental Science and Technology is a RoMEO green journal. This permits authors to archive any version of their article they find most suitable, including the published version on their institutional repository and any other suitable website.

Please see http://www.sherpa.ac.uk/romeo/search.php?issn=1684-5315

Digital Archiving Policy

The African Journal of Environmental Science and Technology is committed to the long-term preservation of its content. All articles published by the journal are preserved by Portico. In addition, the journal encourages authors to archive the published version of their articles on their institutional repositories and as well as other appropriate websites.

https://www.portico.org/publishers/ajournals/

Metadata Harvesting

The African Journal of Environmental Science and Technology encourages metadata harvesting of all its content. The journal fully supports and implement the OAI version 2.0, which comes in a standard XML format. See Harvesting Parameter

Memberships and Standards

Academic Journals strongly supports the Open Access initiative. Abstracts and full texts of all articles published by Academic Journals are freely accessible to everyone immediately after publication.

All articles published by Academic Journals are licensed under the Creative Commons Attribution 4.0 International License (CC BY 4.0). This permits anyone to copy, redistribute, remix, transmit and adapt the work provided the original work and source is appropriately cited.

Crossref is an association of scholarly publishers that developed Digital Object Identification (DOI) system for the unique identification published materials. Academic Journals is a member of Crossref and uses the DOI system. All articles published by Academic Journals are issued DOI.

Similarity Check powered by iThenticate is an initiative started by CrossRef to help its members actively engage in efforts to prevent scholarly and professional plagiarism. Academic Journals is a member of Similarity Check.

CrossRef Cited-by Linking (formerly Forward Linking) is a service that allows you to discover how your publications are being cited and to incorporate that information into your online publication platform. Academic Journals is a member of CrossRef Cited-by.

Academic Journals is a member of the International Digital Publishing Forum (IDPF). The IDPF is the global trade and standards organization dedicated to the development and promotion of electronic publishing and content consumption.

Contact

Editorial Office: ajest@academicjournals.org

Help Desk: helpdesk@academicjournals.org

Website: http://www.academicjournals.org/journal/AJEST

Submit manuscript online http://ms.academicjournals.org

Academic Journals
73023 Victoria Island, Lagos, Nigeria
ICEA Building, 17th Floor,
Kenyatta Avenue, Nairobi, Kenya.

Editors

Dr. Guoxiang Liu
Energy & Environmental Research Center
(EERC)
University of North Dakota (UND)
North Dakota 58202-9018
USA

Prof. Okan Külköylüoglu
Faculty of Arts and Science
Department of Biology
Abant Izzet Baysal University
Turkey.

Dr. Abel Ramoelo
Conservation services,
South African National Parks,
South Africa.

Editorial Board Members

Dr. Manoj Kumar Yadav
Department of Horticulture and Food
Processing
Ministry of Horticulture and Farm Forestry
India.

Dr. Baybars Ali Fil
Environmental Engineering
Balikesir University
Turkey.

Dr. Antonio Gagliano

Department of Electrical, Electronics and
Computer Engineering
University of Catania
Italy.

Dr. Yogesh B. Patil
Symbiosis Centre for Research & Innovation
Symbiosis International University
Pune,
India.

Prof. Andrew S Hursthouse
University of the West of Scotland
United Kingdom.

Dr. Hai-Linh Tran
National Marine Bioenergy R&D Consortium
Department of Biological Engineering
College of Engineering
Inha University
Korea.

Dr. Prasun Kumar
Chungbuk National University,
South Korea.

Dr. Daniela Giannetto
Department of Biology
Faculty of Sciences
Mugla Sitki Koçman University
Turkey.

Dr. Reem Farag
Application department,
Egyptian Petroleum Research Institute,
Egypt.

Table of Content

Vol. 17(11), pp. 275-293, November 2023
DOI: 10.5897/AJEST2023.3222
Article Number: 314D05471456
ISSN: 1996-0786
Copyright ©2023
Author(s) retain the copyright of this article
http://www.academicjournals.org/AJEST

ACADEMIC JOURNALS
expand your knowledge

African Journal of Environmental Science and Technology

Full Length Research Paper

Assessment of the LMDZ model to the dynamic and thermodynamic properties of cyclogenesis in the tropical Atlantic Ocean and on the West African coast

Dame Gueye[1], Abdou Lahat Dieng[2], Abdoulaye Deme[1]*, Mouhamadou Bamba Sylla[3] and Abdou Aziz Coly[1]

[1]LEITER, Applied Science and Technology Training and Research Unit, Gaston University, BP 234, Saint-Louis 32000, Senegal.
[2]LPAOSF, Polytechnic School, Cheikh Anta Diop University, BP 5085, Dakar 10700, Senegal.
[3]African Institute for Mathematical Sciences (AIMS), KN3 Street Kigali, Rwanda.

Received 15 August, 2023; Accepted 23 October, 2023

The study's primary objective is to evaluate the LMDZ model's capacity to simulate the cyclogenesis process, interannual variability of cyclone activity, and associated processes in the tropical Atlantic, focusing on the West African coasts to the central tropical Atlantic region. Two main approaches are used. Firstly, the model's ability to capture the interannual variability in Atlantic cyclogenesis activity is examined through seasonal mean. These seasonal average conditions were identified based on ERAI, along with years characterized by strong and low cyclonic activities. Secondly, a more descriptive approach is undertaken, involving the spatiotemporal monitoring of the Hurricane Karl, which originated near the Cape Verdean coasts on September 16th, 2004, until its dissipation. Horizontal sections of the tropospheric layers most sensitive to the cyclonic phenomenon are used to comprehensively track its progress. The results show a significant variability of cyclonic activity in the tropical Atlantic at different time scales, indicating that the period from July to September and the region along the Intertropical Convergence Zone (ITCZ) are favorable for tropical cyclogenesis. It also revealed that the years of high cyclonic activity are mainly characterized by low sea level pressure, strong 850 hPa relative vorticity, high 700 hPa relative humidity, and strong 200 hPa divergence anomalies, whereas the opposite is observed during the low activity years. The LMDZ model performs well in reproducing cyclonic parameters from the surface to the upper troposphere with mean absolute errors being less important from the surface (11%) to the high troposphere (17%). At the synoptic scale, the model accurately replicates hurricane characteristics, including intensity categories, spatial distribution, and trajectories. However, it falls short in accurately representing the genesis phase, such as tropical depression.

Key words: Cyclogenesis, interannual variability, cyclonic activity, tropical depression.

INTRODUCTION

The troposphere, the lowest layer of earth's atmosphere, where various meteorological events like fog, thunderstorms, tornadoes, and cyclones occur. While these events are essential for providing precipitation for human activities, they can also pose significant public danger.

Tropical cyclones, highly destructive natural disasters causing significant human and property loss, rely on specific conditions for their formation. These cyclones usually originate near the intertropical convergence zone (ITCZ), characterized by low pressure, where trade winds from different hemispheres converge. Notably, in the tropical Atlantic, major cyclones (Category 3 to 5) account for more than 70% of natural damage in the United States (Landsea, 1993).

They can then cause loss of life and property when they evolve near the coast. For example, Hurricane Katrina in 2005 was one of the strongest hurricanes in US history, resulting in approximately 1,836 deaths and causing damage estimated at more than $108 billion. In Senegal, Tropical Storm Cindy led to the death of several Senegalese fishermen in 1999 (Sall and Sauvageot, 2005). More recently, hurricane Fred, which passed through the Cape Verde Islands in 2015, caused damage on seven out of ten islands and also affected Senegal's coastline, resulting in fatalities associated with a fishing vessel (Jenkins et al., 2017).

The intensification of hurricanes, coupled with their higher frequency due to climate change (Goldenberg et al., 2001), underscores the growing impact of these storms. Climate change is increasingly recognized for amplifying hurricane strength and their capacity for increased rainfall, posing a significant threat to vulnerable regions. To mitigate the far-reaching consequences, our primary defences include observation, understanding, forecasting, and early warning systems. Progress in these areas is vital for more effective planning, risk reduction, and the protection of human lives and property. Climate models, offering reliability, play a pivotal role in advancing these efforts.

Climate models play a crucial role in understanding earth's climate and predicting future climate changes. They incorporate the laws of physics, chemistry, and fluid dynamics, including interactions between the ocean, atmosphere, and surfaces at different time and space scales that significantly impact climate sensitivity (Pohl, 2017). LMDZ is an atmospheric general circulation model (GCM) developed by the ‘Laboratoire de Météorologie Dynamique’ (LMD, where "Z" refers to the regional refinement capability of the grid or Zoom) of ‘Centre National de la Recherche Scientifique’ (CNRS). It is used as the atmospheric component of the integrated earth system model at ‘Institut Pierre Simon Laplace’ (IPSL). The model contributes significantly to the climate change projections used to inform Intergovernmental Panel on Climate Change (IPCC) reports (Hourdin et al., 2006). The simulations used in this study are simulations with the new physic version of the LMDZ model (LMDZ5). These simulations are used in model intercomparison projects, namely the Atmospheric Model Intercomparison Project (AMIP), which tests all the parameterizations coupled to large-scale dynamics.

Multiple research studies have explored the LMDZ model's performance in West Africa, particularly in various aspects of atmospheric physics. For example, Senghor et al. (2017) delved into the processes governing Saharan dust's vertical distribution. Their work contributed to quantifying the impact of different mechanisms on the seasonal variations of mineral particle distribution in West Africa and the Tropical Atlantic Ocean. The LMDZ model played a pivotal role in identifying the primary physical drivers behind the distinct seasonal patterns in surface dust concentrations and integrated column concentration cumulants. Diallo (2012) focused on understanding the interactions between atmospheric and surface convection and how they influence energy balances. Through both unconstrained and guided simulations, they established feedback connections between convection and monsoon circulation. Additionally, within the "Analyse Multidisciplinaire de la Mousson Africaine" (AMMA) campaign in West Africa, Sane (2011) sets out to assess and validate new model parameterizations, particularly in their ability to represent the life cycle of convective systems. This encompassed dynamic facets of the monsoon, cloud formations, and rainfall patterns. Results indicated that the model effectively mirrored the diurnal cycle of local systems, resembling observed diurnal patterns. However, it fell short in replicating the propagation of convective systems. Furthermore, recent research employing high-resolution GCMs different to LMDZ, has explored cyclone reproduction, forecasting, and climate simulation. These studies (Ohfuchi et al., 2004; Shen et al., 2006; Chauvin et al., 2006; Oouchi et al., 2006) have demonstrated the models' capacity to accurately replicate the intricate circulation patterns and the intensity of tropical cyclones.

In light of the LMDZ model's demonstrated success in various domains, it becomes pertinent to extend its evaluation to more complex phenomena, particularly with regards to cyclonic activity variability and related processes. These intricate facets present a substantial challenge, distinct from the previously explored topics. They offer a rigorous examination of the model's capabilities and its potential utility in comprehensive climate research. Furthermore, they provide insights into representing cyclonic systems across synoptic and mesoscale dimensions, along with the features of the

*Corresponding author. E-mail: abdoulaye.deme@ugb.edu.sn. Tel: +221-764149737.

Author(s) agree that this article remain permanently open access under the terms of the Creative Commons Attribution License 4.0 International License

West African Monsoon.

Motivated by these considerations, this study aims to assess the LMDZ model's performance in simulating cyclogenesis, cyclonic activity variability, and the associated processes spanning from the West African coasts to the tropical Atlantic basin. The study first delves into the model's ability to replicate West African cyclonic activity across the open Atlantic Ocean. Subsequently, it conducts a brief analysis of the mean conditions during the tropical Atlantic cyclone season, comparing periods of high and low cyclone activity to evaluate the model's proficiency in representing mean conditions and key aspects of the West African Monsoon (WAM). Finally, the study encompasses a space-time analysis of meteorological parameters linked to the progression of tropical cyclone Karl.

EXPERIMENTAL

Validation data

Reanalyses

Reanalysis involves merging data from various sources, including ground measurements, radiosondes, and satellite observations, with a weather forecasting model. The result is an extensive database of atmospheric and oceanic variables, covering global scales and ranging from short-term to long-term temporal resolutions. These datasets, known as reanalyses, offer a thorough and consistent representation of the earth's climate system (Dieng, 2015). We have chosen to validate the model against ERA-Interim reanalyses from the European Center for Medium-Range Weather Forecasts (ECMWF) for a period from 1979 to 2009. According to Dee et al. (2011), ERAI (ECMWF Re-Analysis Interim) is a frequently used global atmospheric reanalysis.

Observation

The NHC (National Hurricane Center) is the specialized institution responsible for monitoring and issuing warnings about cyclones in the North Atlantic and Eastern Pacific regions. At the conclusion of each cyclone season, the NHC compiles maps that contain detailed information about each cyclone. This information typically includes the cyclone's lifespan, date of formation, its position and intensity recorded at 6-h intervals, minimum pressure, maximum wind speed, and any associated material or human damage caused by the cyclone (Weinkle et al., 2018). These data sets from the NHC were utilized for a statistical study to analyse the temporal variability of cyclone activity. The study covered a period from 1979 to 2009 and focused on cyclone activity in the North Atlantic region.

Tools

The LMDZ model

Operating principle and basic discretized equations on the sphere: LMDZ, specifically, is an atmospheric General Circulation Model (GCM) known for its substantial contribution to climate change projections featured in the reports of the IPCC (Hourdin et al., 2006). It solves the primitive equations through its dynamic core module (Baek et al., 2014). Solving the basic equations of atmospheric dynamics involves a number of approximations and simplified versions for the study of atmospheric and even oceanic general circulation. These approximations primarily pertain to the thin-film approximation, which assumes that optical thickness is insignificantly small compared to the earth's radius, and the hydrostatic approximation.

1) Conservation of mass

$$\frac{D\rho}{Dt} + \rho div U = 0 \quad (1)$$

2) Conservation of potential temperature

$$\frac{D\theta}{Dt} = \frac{Q}{Cp}\left(\frac{Po}{P}\right)^{k} \quad (2)$$

3) Conservation of momentum

$$\frac{DU}{Dt} + \frac{1}{\rho} - g + 2\Omega \wedge U = F \quad (3)$$

4) Conservation of secondary components

$$\frac{Dq}{Dt} = Sq \quad (4)$$

where U = $u\vec{i} + v\vec{j} + w\vec{k}$ represents the three-dimensional wind vector (m/s), ρ the density of dry air (kg/m^3), P the air pressure (Pa), g gravity (m/s^2), and Ω the angular velocity of the earth's rotation (s^{-1}).

The LMDZ5 "New physics": LMDZ5 is the current version of the LMDZ atmospheric general circulation model (Hourdin et al., 2006) which is used for climate studies, climate change projections, and environmental studies. LMDZ5 is the atmospheric component of the IPSL Coupled Model (IPSL-CM5) used in particular for climate change projections in the frame of CMIP5. It introduces several improvements to its physics components, including a new boundary layer scheme that combines a turbulent diffusion model with a prognostic equation for turbulent kinetic energy, following approach. It also incorporates a "mass flow" scheme to represent coherent dry convective structures and cloud boundary layer structures described by Rio and Hourdin (2008). Furthermore, the model integrates a modified version of the Emanuel thunderstorm convection scheme, with changes in mixing probability prescriptions, closure mechanisms, and triggering criteria based on boundary layer characteristics, as outlined by Rio et al. (2009). The convection scheme is coupled with a parameterization addressing the formation of cold pockets from convective rain re-evaporation, influencing convection initiation and termination. These enhancements collectively refine the model's representation of complex atmospheric processes.

Methods

In this research, the study focuses on identifying the environmental conditions conducive to cyclogenesis, the process of cyclone formation. To achieve this, horizontal sections of various atmospheric layers are analysed. This approach helps in pinpointing the essential requirements, including both dynamic and thermodynamic conditions that support the development of

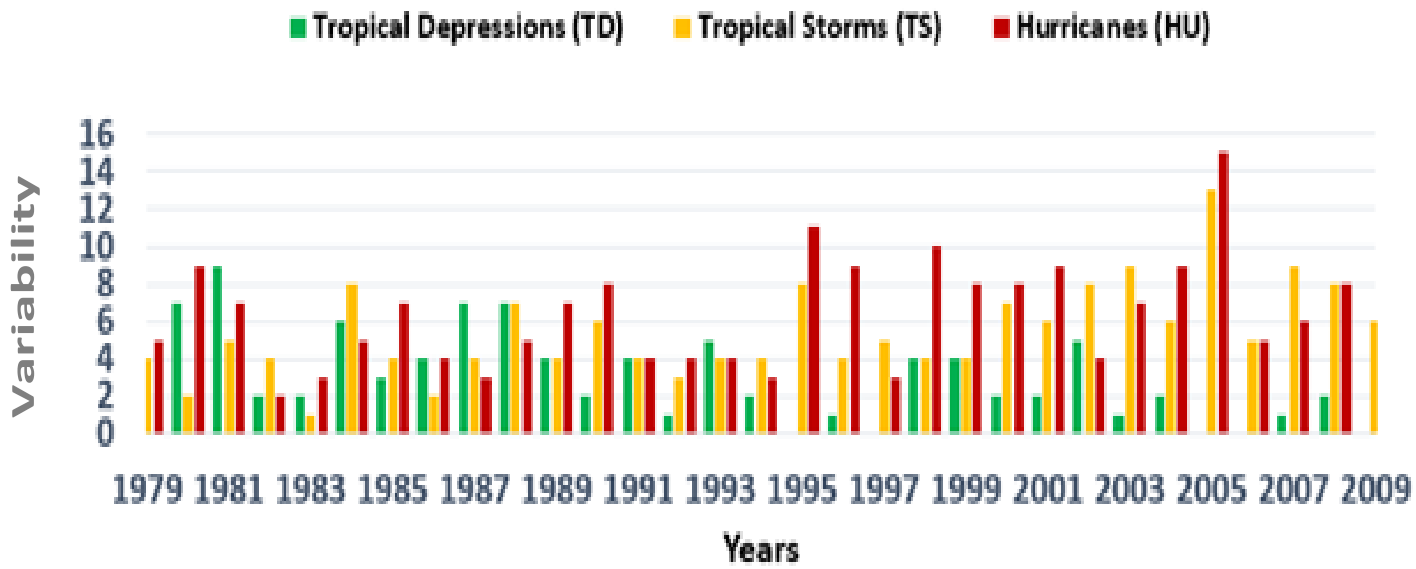

Figure 1. Interannual variability of cyclonic activity in the North Atlantic from 1979 to 2009.

cyclones. It also helps in identifying specific geographic regions and favorable time periods, such as July, August, and September (JAS), when cyclonic activity tends to be most prevalent.

The research begins with a statistical analysis of cyclone activity using data from the NHC archive. In this study, a tropical cyclone in the Atlantic basin is defined as an atmospheric disturbance that progresses through the stages of Tropical Depression (TD), Tropical Storm (TS), and hurricane (HU) in succession.

To assess cyclonic activity, we focus on the parameter "frequency," which refers to the annual count of TDs, TSs, and HUs observed from 1979 to 2009 (Figure 1). This approach allows for the identification of years with high activity years (HAY) and low activity years (LAY) in the Atlantic basin. These seasons are determined based on the interannual variability (Figure 1), where the average number of cyclonic activities and the standard deviation are calculated.

LAY are defined as those with a cyclonic activity count below μ - σ, where μ represents the average annual number of cyclonic activities calculated from 1979 to 2009, and σ is the associated standard deviation. In this context, LAY corresponds to the years 1982, 1983, 1987, 1994, 1997, and 2009. On the other hand, HAY are those with a cyclonic activity count exceeding μ + σ. HAY in this study includes 1980, 1995, 1996, 1998, 2001, 2004, and 2005. These categorizations provide a basis for further analysis and investigation into the factors influencing cyclonic activity in the Atlantic basin.

The next step in the research involves conducting a composite analysis for the years of both high cyclonic activity (HAY) and low cyclonic activity (LAY) using the ERAI reanalysis dataset. The goal is to identify and understand the average seasonal patterns associated with these particular years. The comparison between the two average conditions of reanalysis and simulations will show us how well LMDZ captures the atmospheric conditions during these periods. Then, the 850 and 200 hPa relative vorticity and divergence are calculated from the ERAI wind data. These parameters are essential for understanding the dynamics and circulation patterns in the atmosphere during HAY and LAY years.

In the final phase of the research, a specific case study focuses on a synoptic-scale disturbance, particularly Hurricane Karl. The objective is to conduct a detailed examination and comparison of this specific weather event. First of all, regarding this study case, a spatiotemporal tracking of hurricane Karl is done. This is accomplished by monitoring the minimum sea level pressure (SLP) associated with the system at 12 h intervals from September 16th to September 23rd. This tracking allows for a comprehensive understanding of the hurricane's movement and development over time.

The instantaneous speed of the disturbance and the average speed of translation were then calculated. To do this, the Haversine formula is used to calculate the distance between each two geographical points (longitude and latitude) on a sphere, such as the earth. This formula is particularly useful for determining distances on a sphere, such as the earth. It takes into account the curvature of the earth's surface when measuring distances between points. Here is the Haversine formula:

$$a = sin^2(\frac{\Delta lat}{2}) + \cos(lat1) \times \cos(lat2) \times sin^2(\frac{\Delta lon}{2}) \quad (5)$$

$$c = 2 \times \text{atan2}(\sqrt{a}, \sqrt{(1-a)}) \quad (6)$$

$$distance = R \times c \quad (7)$$

where Δlat is the difference in latitude between the two points, Δlon is the difference in longitude between the two points, lat1 and lat2 are the latitudes of the two points, respectively. R is the radius of the sphere (for example, the average radius of the earth in meters).

To provide a more comprehensive understanding of the spatiotemporal evolution of Hurricane Karl, several additional tools and techniques are utilized.

Hovmöller diagram of relative vorticity (850 hPa)

A Hovmöller diagram is created to visualize the spatiotemporal

evolution of relative vorticity at the 850 hPa level. This diagram is divided into two phases:

1) Zonal tracking (September 16 to 19th): Relative vorticity is averaged over latitudes between 10 and 20°N. This provides a zonal (East-West) perspective of the hurricane's behaviour during this period.
2) Meridional Tracking (September 20th to 23rd): Relative vorticity is averaged over longitudes between 50° and 45°W. This offers a meridional (North-South) view of the hurricane's characteristics during this phase.

Daily anomalies of horizontal cross-section structures

Daily anomalies are constructed to examine the horizontal cross-sectional structures associated with Hurricane Karl. These anomalies provide insights into how the hurricane's characteristics and structure change from its genesis, development to its dissipation. The analysis typically spans from the earth's surface to the upper troposphere, allowing for a comprehensive assessment of the hurricane's development. The data was processed, and the calculations were performed using Anaconda (Python) software in the Spyder environment.

RESULTS AND DISCUSSION

Climatology of seasonal average conditions

On the surface (SLP and wind)

Figure 2 shows the JAS seasonal mean of Sea Level Pressure (SLP, colours) and 10 m wind patterns (vectors) for ERA Interim (left) and LMDZ (right). In the ERA-Interim dataset (Figure 2a), the lowest SLP values are observed between the equator and latitude 14°N. This observation aligns with expectations, as this region corresponds to the Intertropical Convergence Zone (ITCZ), which typically extends from 8 to 17°N. The ITCZ is known as a key area where many tropical depressions originate (DeMaria et al., 2001). Around this latitude band, the north-easterly and south-westerly trade winds converge, as shown in Figure 2a. Figure 2b illustrates that, compare to ERAI, the LMDZ model captures the broad features of SLP and wind patterns during the JAS period but exhibits a slight overestimation of SLP intensity in certain regions, particularly in the Gulf of Guinea. The mean absolute error (MAE) between the model and observations indicates an error percentage of approximately 11%.

Anomalies associated with the season of high activity (HAY) and those of low activity (LAY) are presented in Figure 3. The HAY (LAY) is associated with a negative (positive) SLP anomaly in the north-western part of the Atlantic (Figure 3a and c). This area of lower SLP encompasses the north-western part of the MDR (Main Development Region), an area known for highly favorable meteorological conditions for cyclone formation. The wind surface anomaly exhibits a cyclonic structure, centered on the area of lowest SLP in HAY (Figure 3a) and anticyclonic structure in LAY (Figure 3c).

These patterns are respectively consistent with the circulation expected during active cyclone and less active cyclone seasons. The model successfully reproduces these observed anomalies associated with HAY and LAY.

However, it is noted that the model tends to overestimate the SLP anomalies in the Gulf of Guinea region. Overall, these findings indicate that the model captures the essential features of SLP and wind patterns during high and low cyclonic activity years, providing valuable insights into the atmospheric dynamics associated with different cyclone seasons.

In the lower troposphere (850 hPa - relative vorticity and wind)

Figure 4 shows the climatology at 850 hPa of the relative vorticity (s^{-1}, in colour) and the horizontal wind patterns (m. s^{-1}, in vector) and the anomalies associated with seasons of high and low cyclonic activity (Figure 5).

On the continent, a positive relative vorticity is located on either side of the 15°N latitude (Figure 4a). According to Diedhiou et al. (2001) and Fink and Reiner (2003), these structures correspond to the trajectories of African Easterly Waves (AEW) propagating north and south of the African Easterly Jet (AEJ). The southern AEWs, deriving energy from the AEJ, are located in the humid zone and play a role in modulating rainfall in West Africa (Pytharoulis and Thorncroft, 1999; Chen, 2006). The northern AEWs are favored by baroclinic energy conversions (Burpee, 1972; Diedhiou et al., 1999). The two wave paths merge over the Atlantic Ocean, in the ITCZ, where most tropical depressions also originate (Figure 4a). Indeed, a positive vorticity is a necessary parameter for cyclogenesis in the basin. Winds converge toward the ITCZ, slowing down over land due to friction. The LMDZ model simulates the spatial distribution of vorticity fields, highlighting the trajectories of southern and northern AEWs. However, it tends to underestimate the vorticity intensity in the ITCZ and along both AEW paths (Figure 1b). The mean absolute error (MAE) between the observed and model vorticity fields is approximately 12%.

In HAY, positive vorticity anomalies are observed in the western oceanic zone, above 15°N and 30°W, accompanied by cyclonic wind circulation (Figure 5a). Over the continent, positive vorticity anomalies reflect the activity of northern AEWs north of the AEJ, with a cyclonic circulation in the Saharan Air Layer (SAL). However, negative vorticity is noted in the same area during LAY (Figure 5c) with an anticyclonic wind circulation. Thus, the southern AEWs are more active during LAY, indicating the enhanced activity of southern

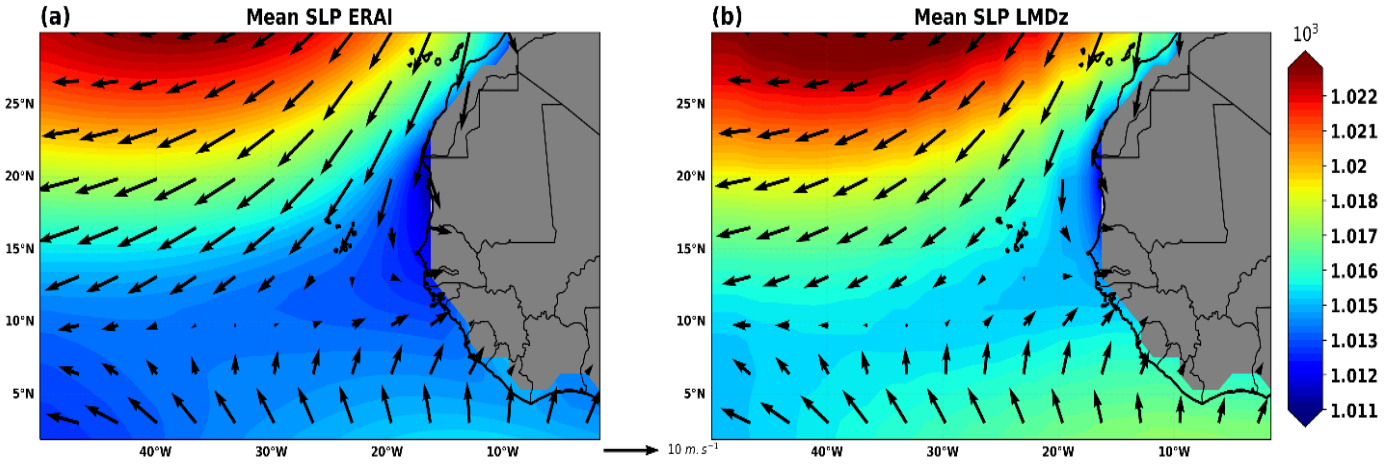

Figure 2. Seasonal average (July-September from 1979 to 2009) of SLP (hPa, in colour) and average horizontal wind at 10 m (m. s^{-1}, in vector) for ERA Interim (a) and LMDZ model (b).

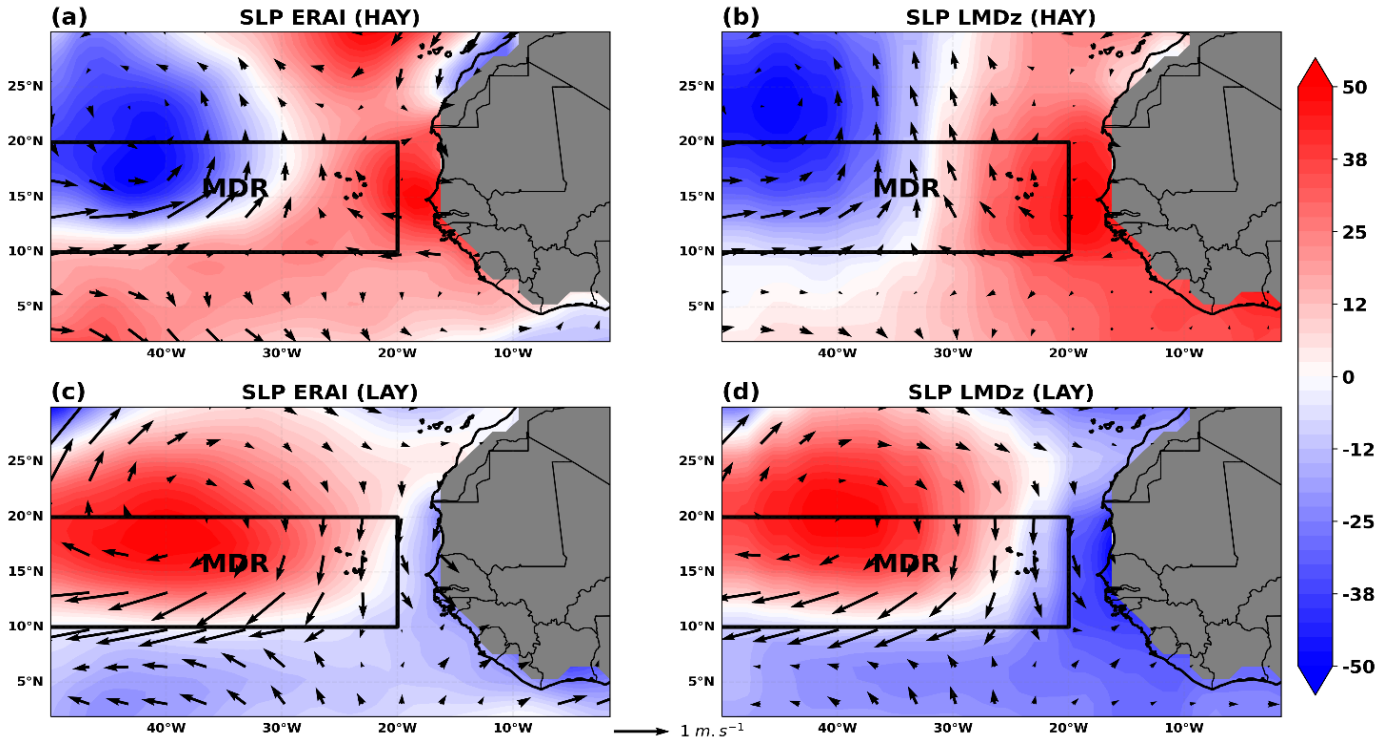

Figure 3. Seasonal anomalies of SLP (10^{-2} hPa, in colour) and horizontal wind (m. s^{-1}, in vector) for HAY (top) and LAY (bottom) for ERA Interim (a, c) and LMDZ (b, d).

AEWs. The model reproduces these patterns, including the distribution of relative vorticity anomalies and AEW activity in HAY and LAY (Figure 2d). Similarly, the model replicates the trends in the wind field anomalies at 850 hPa.

In the mid-troposphere (700 hPa - relative humidity and wind)

Globally, areas with high humidity (>70%) in the seasonal averages are concentrated between the equator and

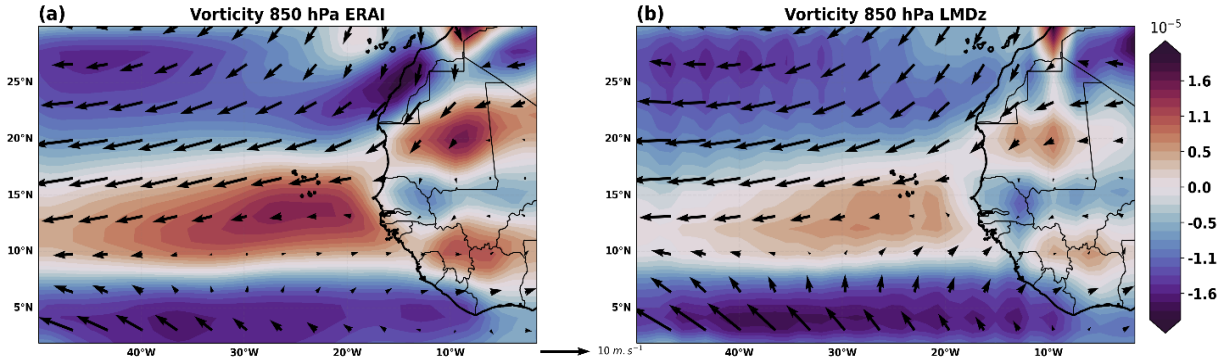

Figure 4. Seasonal average (July-September from 1979 to 2009) of relative vorticity (s^{-1}, in colour) and average horizontal wind (m. s^{-1}, in vector) at 850 hPa for ERA Interim (a) and LMDZ model (b).

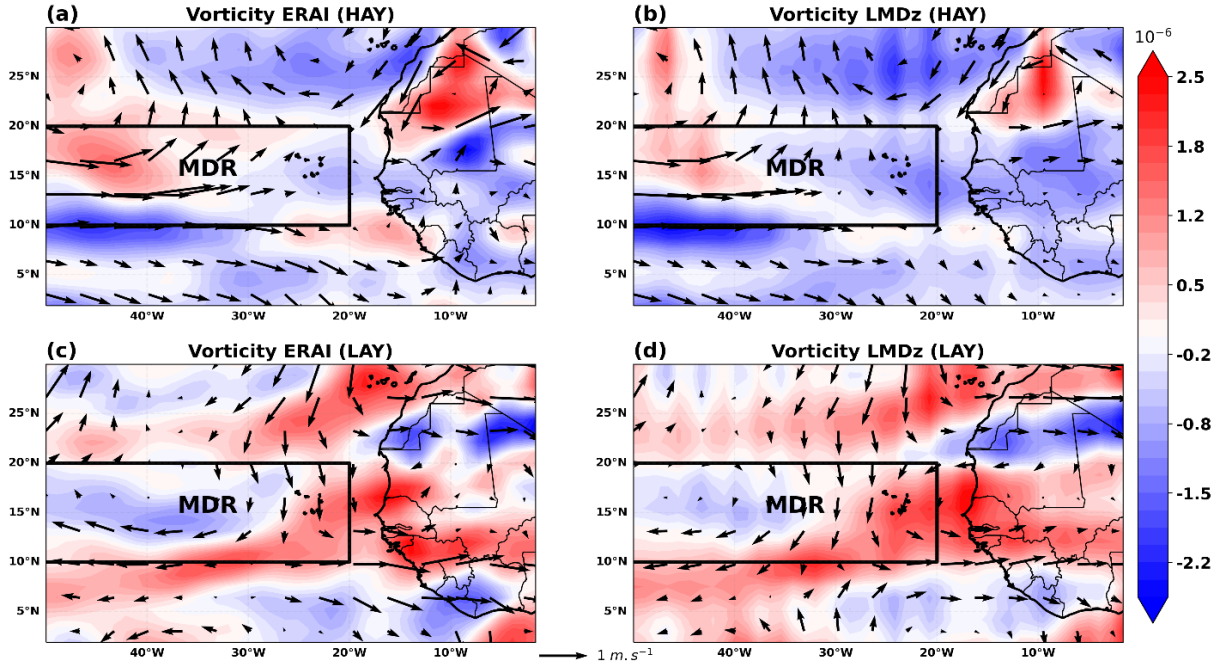

Figure 5. Seasonal anomalies of relative vorticity (s^{-1}, in colour) and horizontal wind (m. s^{-1}, in vector) at 850 hPa for HAY (top) and LAY (bottom) for ERA Interim (a, c) and LMDZ (b, d)).

14°N (Figure 6a), corresponding to the ITCZ area. The circulation at 700 hPa is influenced by the African Easterly Jet (AEJ), with its maximum speed typically between 12°N and 18°N varying around 12 m.s^{-1}. Maxima in relative humidity were observed just south of the AEJ. The LMDZ model is capable of representing the seasonal average of relative humidity (Figure 6b), which closely resembles the ERA-Interim reanalysis data. However, the model tends to overestimate relative humidity, particularly in the 5 to10°N latitude band. The mean absolute error (MAE) between observations and the model indicates a 14% error in relative humidity at 700 hPa.

A positive anomaly was found (Figure 7a) in the zone covering the entire MDR area during HAY. Thus, this moisture is crucial at this level and is synonymous with high-water content that helps resist downdrafts. In addition, a wind anomaly with a cyclonic circulation is noted in the positive relative humidity anomaly area. The southerly winds are accelerated with a slowing of the AEJ off the basin as well as acceleration to the East of the basin. In contrast to the HAY, LAY is associated with a negative anomaly (Figure 7c) in relative humidity, with an

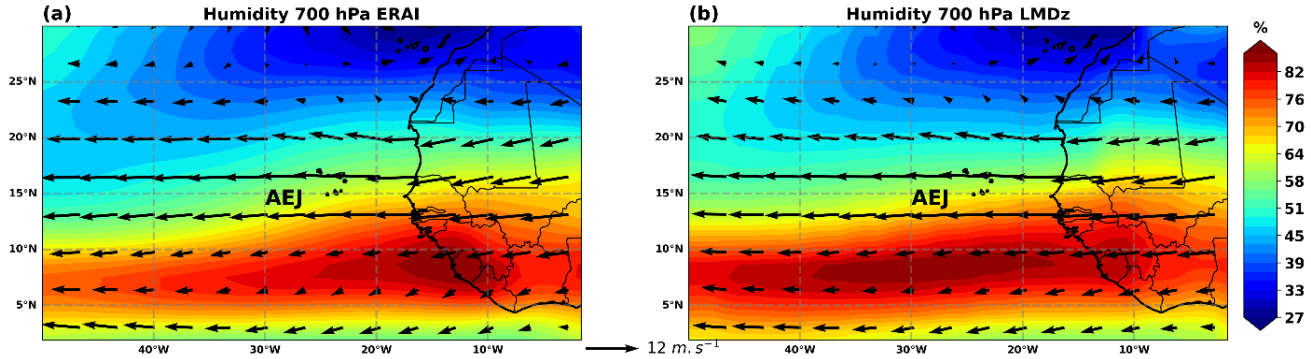

Figure 6. Seasonal average (July-September from 1979 to 2009) of relative humidity (%, in colour) and average horizontal wind (m. s^{-1}, in vector) at 700 hPa for ERA Interim (a) and LMDZ model (b).

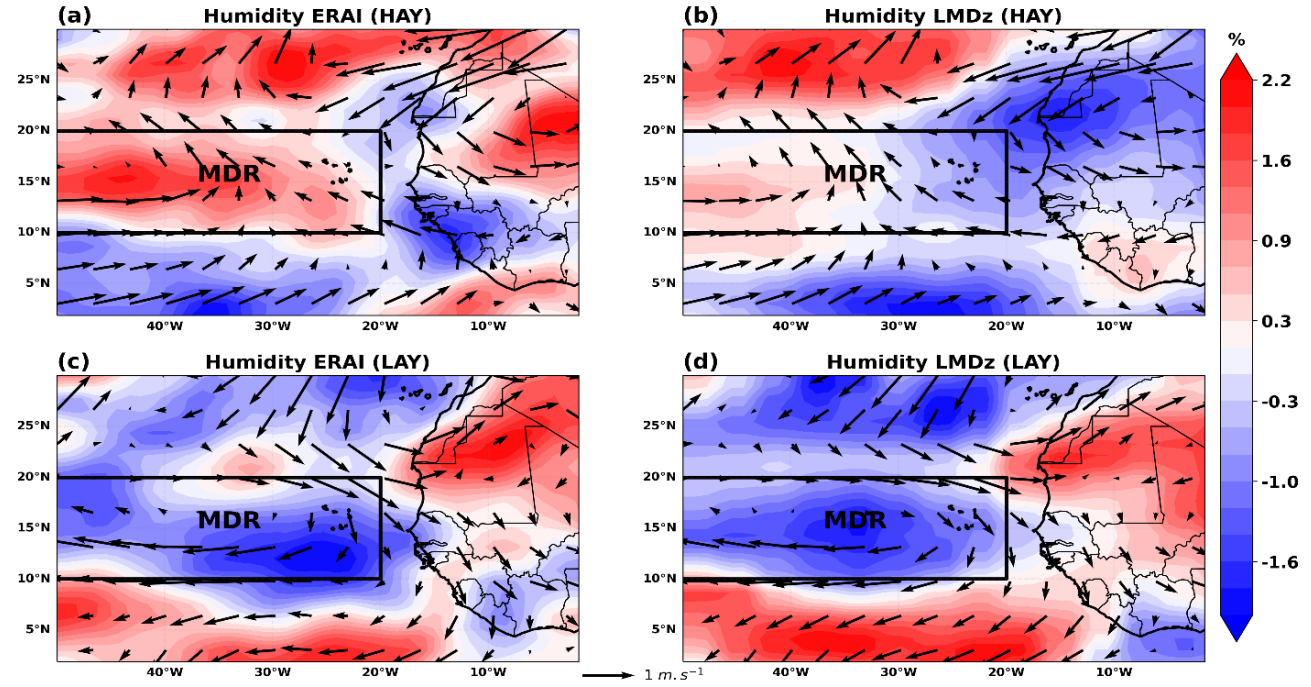

Figure 7. Seasonal anomalies of relative humidity (%, in colour) and horizontal wind (m. s^{-1}, in vector) at 700 hPa for HAY (top) and LAY (bottom) for ERA Interim (a, c) and LMDZ (b, d)).

anticyclonic circulation of winds. These conditions are synonymous with a drying of the middle troposphere, which favours downward movements that are not conducive to maintaining the disturbance. Wind patterns in LAY show behaviour opposite to that of HAY.

The findings emphasize the importance of relative humidity in the middle troposphere as a critical factor for cyclone genesis in the tropical Atlantic. The LMDZ model successfully reproduces the different relative humidity structures in the basin during HAY and LAY, while capturing the behaviour of the AEJ for each season.

In the upper troposphere (200 hPa - divergence and wind)

The analysis of the atmosphere at the 200 hPa level, which includes features like the Tropical Easterly Jet (TEJ, with wind speeds around 16 m/s) and Subtropical Westerly Jet (JOST, with wind speeds around 18 m/s), provides valuable insights into the West African Monsoon (WAM) and its relationship with cyclonic activity. These opposing zonal flows exist between 5-10°N and 24-30°N, respectively (Figure 8a). The ERAI reanalyses exabit a

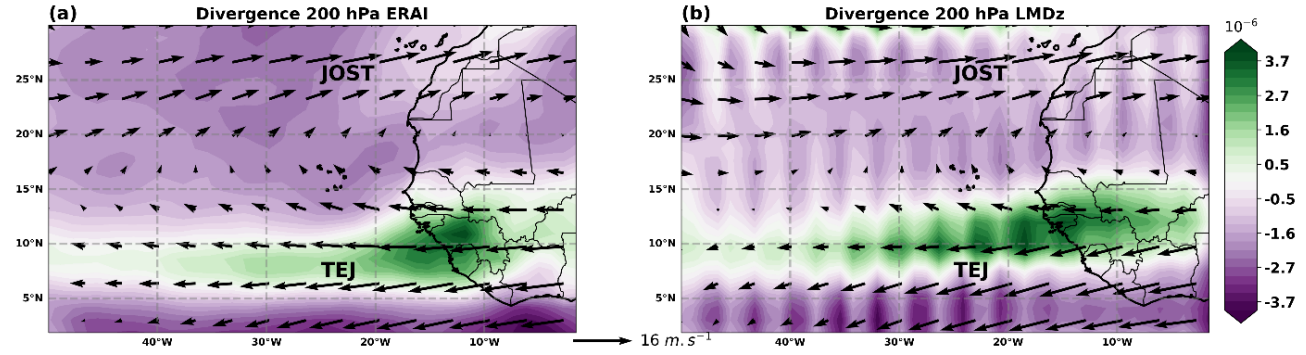

Figure 8. Seasonal average (July-September from 1979 to 2009) of divergence (s^{-1}, in colour) and average horizontal wind (m. s^{-1}, in vector) at 200 hPa for ERA Interim (a) and LMDZ model (b).

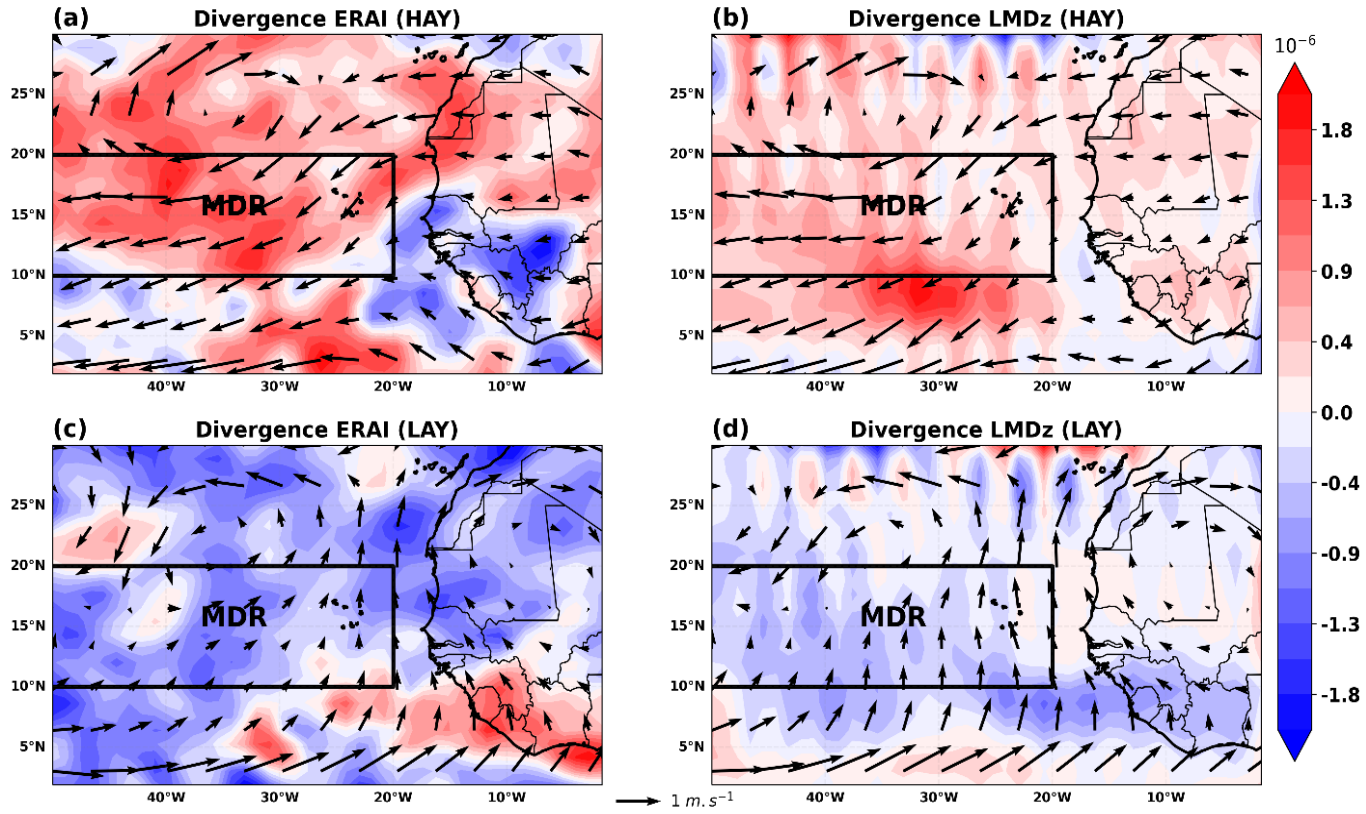

Figure 9. Seasonal anomalies of divergence (s^{-1}, in colour) and horizontal wind (m. s^{-1}, in vector) at 200 hPa for HAY (top) and LAY (bottom) for ERA Interim (a, c) and LMDZ (b, d)).

significant divergence above the ITCZ band, area of maximum relative vorticity and humidity in the low and medium layer (Figures 4a and 6a) and the lowest SLP (Figure 2a). Indeed, the divergence at 200 hPa is essential for the maintenance of the disturbances as it supports the evacuated ascending flows from the surface, thus confirming the results of Chen (2006). The model is able to reproduce the wind field's structure, with intensity similar to the reanalyses and a good spatial distribution of the divergence field in the seasonal mean with a MAE of 17%. However, the model slightly overestimates the seasonal divergence field, especially in the vicinity of the ITCZ band.

HAY is associated with a positive divergence anomaly

and an anticyclonic wind circulation anomaly over the Azores High Pressure (Figure 9a). In contrast to HAY, LAY shows a negative divergence anomaly accompanied by a cyclonic circulation anomaly (Figure 9c). Intense seasons are associated with a weak strengthening of the TEJ while it is strongly slowed down during low activity seasons. This result confirms the work of Camara (2006) who showed that AEWs that develop into tropical cyclones in the Atlantic evolve in an environment with strong TEJ. The LMDZ model successfully reproduces the observed anomaly trends in divergence and wind patterns during HAY and LAY, providing further evidence of the relationship between the West African Monsoon, jet streams, and cyclonic activity in the tropical Atlantic.

In term of the dynamic point on AEWs structures, small differences between the HAY and LAY are noted in the relative vorticity anomaly. This would imply that wave activity plays a minor role in controlling the seasonal variability of cyclogenesis in the tropical Atlantic. However, over the continent, the AEWs north of the AEJ appear to be more active during the HAY. During HAY, it was observed that:

1) A slowdown of the AEJ, especially offshore, associated with a convergence anomaly in the middle layers.
2) A strong acceleration of the TEJ associated with a strong divergence anomaly in the higher layers of the atmosphere.

The combination of the mid-layer convergence anomaly and the high-layer divergence anomaly supports deep convection by strengthening the updrafts. In contrast to the HAY, the LAY are mainly marked by:

1) AEJ acceleration associated with high AEWs activity at 850 hPa.
2) A slowdown of the TEJ associated with a convergence anomaly at 200 hPa.

Here again, the combination of mid-layer relative humidity and divergence anomalies at 200 hPa inhibits convection by favouring subsidence.

Overall, these first results on the seasonal conditions of cyclonic activity in the tropical Atlantic show a good spatial coincidence between the reanalysed and simulated fields. Consequently, the model concedes the ability to represent cyclonic parameters on a climatological scale as well as certain characteristics of the monsoon with more accurate results at the surface than in the upper troposphere. Nevertheless, the model exhibits minor biases in the intensity of the SLP fields, relative vorticity, humidity, and divergence. These discrepancies might be attributed to the parameterization of the model's new version, where the convection scheme is linked to the parameterization of cold pockets formed beneath thunderstorms due to the re-evaporation of convective rainfall, as described by Sane (2011).

Furthermore, several biases are noticeable in the Gulf of Guinea region, which can be attributed to the model's underestimation of low clouds, as indicated by Hourdin et al. (2006), and the fact that this region is prone to convection.

Special case of Atlantic cyclone

Tracks of tropical disturbance associated with Karl

Figure 10 displays the tracks of the tropical disturbance associated with Hurricane Karl from September 16th to 23rd, 2004, in the tropical North Atlantic.

The observations show a translation speed averaging 2.74 $m.s^{-1}$ (Figure 10) from September 16 to 19th. In the simulation, the mean translation speed is 3.05 $m.s^{-1}$ with an instantaneous speed higher than NHC and closer to ERAI (Table 1). In fact, during this period, the model's translation speed is faster than the observations by more than 0.31 $m.s^{-1}$. In other words, for every 100 m traveled by the disturbance in the observations, the model adds 5 m. However, the speed difference between ERAI and LMDZ becomes higher during the track from September 19th to 23rd. During this period, the disturbance slows down to less 0.54 $m.s^{-1}$ in the observations. So, the model reproduces the slowing down of the system during this period, but with less deceleration (0.15 $m.s^{-1}$) than observed. This deceleration of the hurricane-strengthened system may suggest that the intensification of the disturbance fields is causing them to slow down. The trend aligns with a study by Lorck (2019), which showed that as Hurricane Dorian intensified and approached the Bahamas, its forward motion slowed considerably, to less than 0.5 $m.s^{-1}$.

Translation speed

Figures 11 and 12 depict Hovmöller diagrams of the vorticity at 850 hPa, illustrating the westward and northward movement of Hurricane Karl from September 16 to 19th and then from September 20th to 23rd, respectively.

The Hovmöller diagram of the vorticity at 850 hPa shows a disturbance moving westward since its genesis. The tropical depression originated on September 16th near the Cape Verde Islands and developed into a tropical storm the following day. It continued to move westward and intensified into a hurricane on September 18th (Figure 10). The system further evolved and started to move northwards, strengthening into a category 3 major hurricane between September 19 and 20th (Figure 11). It remained a major hurricane, reaching category 4 on the next day. The disturbance maintained its intensity

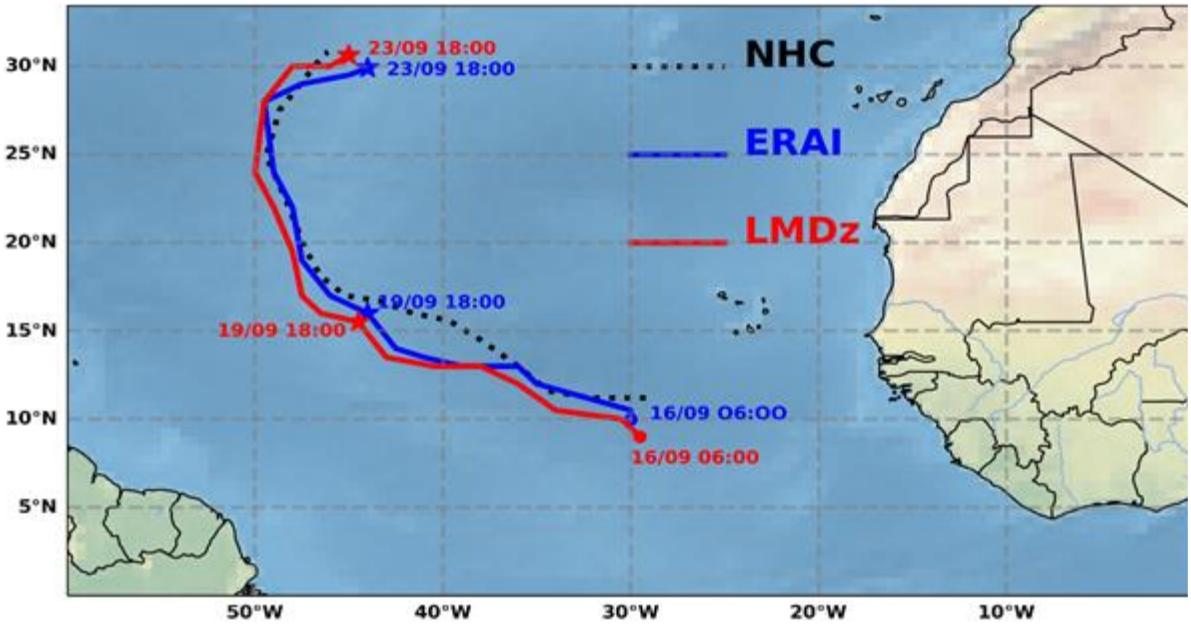

Figure 10. Observed and simulated track at 12h interval of Hurricane Karl from 16th to 23rd September 2004. The dotted line represents the NHC trajectory, ERAI the black line, and LMDZ the red line.

Table 1. Instantaneous speed at genesis's place (29 °W, 11°N) and translation mean speed in $m.s^{-1}$.

Variable	NHC	ERA Interim	LMDz
Instantaneous speed at genesis's place	1.02	1.28	3.61
Translation mean speed from September 16 to 19th	2.18	2.74	3.05
Translation mean speed from September 19th to 23rd	2.08	2.20	2.90

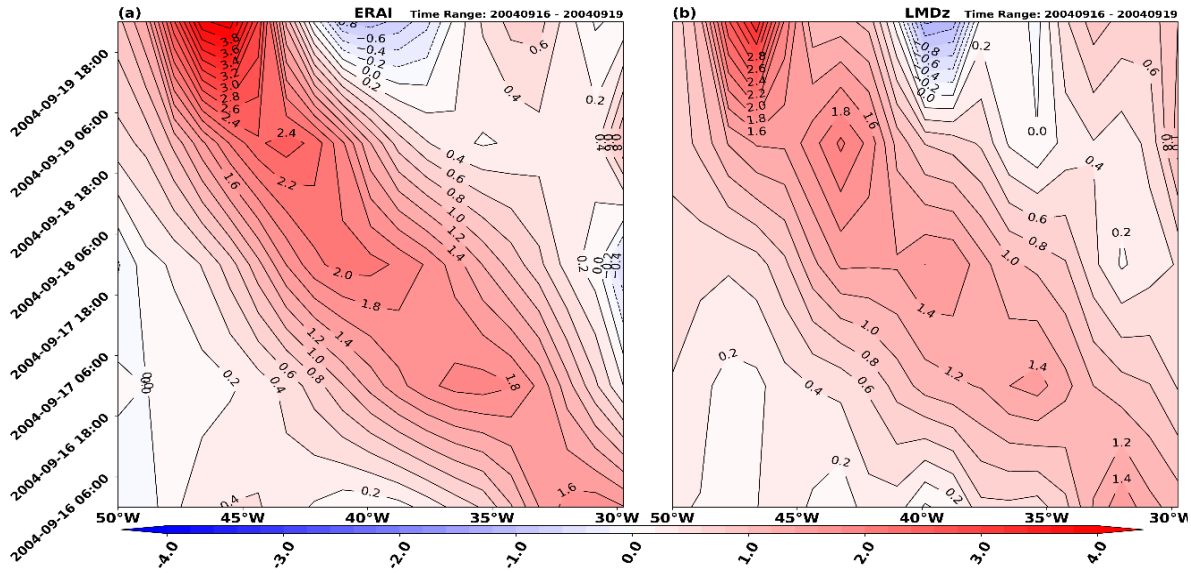

Figure 11. Hovmöller diagram of the vorticity at 850 hPa of ERAI (a) and LMDZ (b) from 16th to 19th September at 12h interval averaged at 10 – 20° N latitudes.

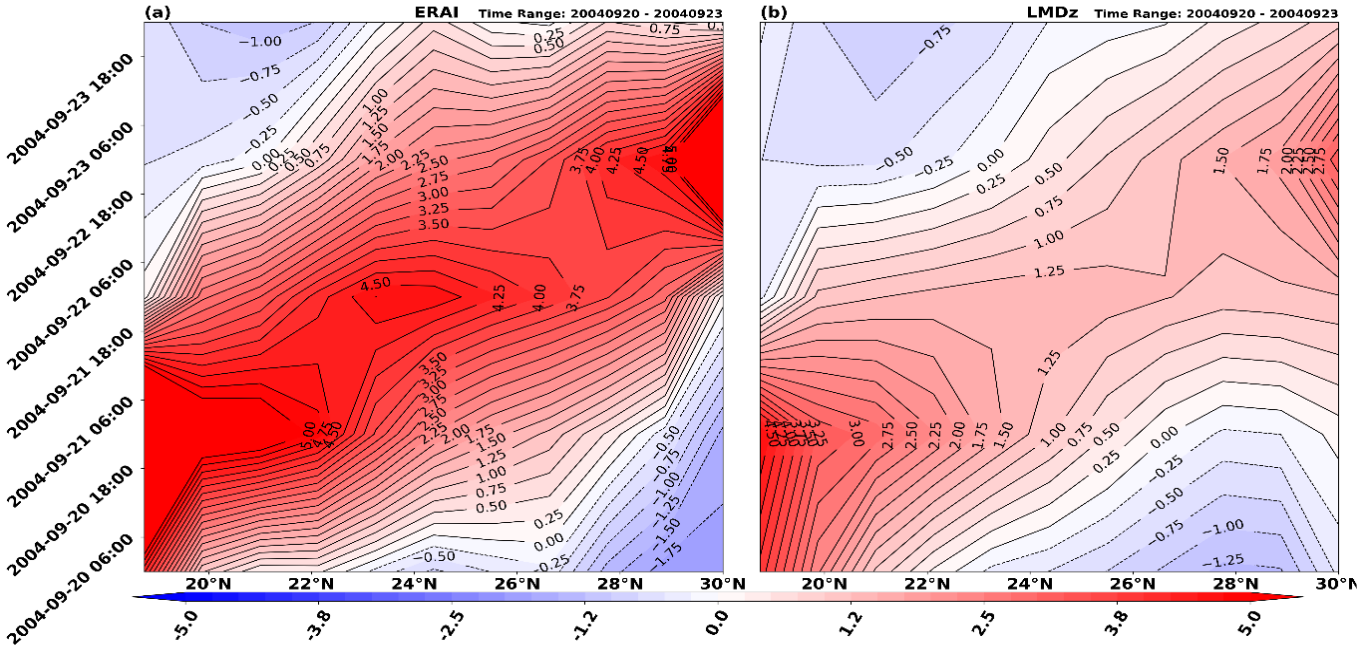

Figure 12. Hovmöller diagram of the vorticity at 850 hPa of ERAI (a) and LMDZ (b) from 20th to 23th September at 12h interval averaged at 50 – 45° W longitudes.

from September 22nd to 23rd and reached a position of 27° North before dissipating on September 24th. Importantly, Hurricane Karl did not pose a threat to any inhabited land. It followed a trajectory toward the northwest and then north, aligning with the results of Beven (2004). The model successfully reproduces the different trajectories of the disturbance as well as the differences in the relative vorticity fields for the various categories of the hurricane.

Evolution of horizontal cross-section structures

On the surface

Figure 13 displays daily anomalies of sea-level pressure (SLP) and surface wind from September 15 to 20th, 2004, showing the evolution of Hurricane Karl.

On the eve of the genesis of the disturbance (September 15th), a vortex circulation progressively sets up toward 10°N, 25°W (Figure 13⋆), which are pre-existing conditions for the genesis of Hurricane Karl (born towards 11°N 29°W). On September 16th, the system was born as a Tropical Depression (TD) and evolved with an increasingly intense and more pronounced cyclonic circulation surrounding a lower SLP. By September 17th, the system had a fairly large negative SLP anomaly and evolved toward the northwest (Figure 13TS), reaching the stage of a Tropical Storm (TS). On the subsequent day (18/09), the disturbance underwent intensification and evolved into a hurricane, exhibiting more distinct cyclonic wind circulation patterns and a negative SLP anomaly (Figure 13HU). Thereafter, it evolves by remaining in the HU stage until it dissipates from the tropics on September 24th. In the simulation, on September 15th, LMDZ does not show signs of pre-existing conditions at Karl's birthplace (11°N, 29°W).

The SLP anomaly becomes negative in the simulation, unlike ERAI, and a cyclonic wind circulation begins to form (TD). However, these conditions are a little late to set up compared to those of ERAI where they are more structured at this stage. At the TS stage, the system is still less intense and less developed in terms of wind circulation and SLP anomaly. However, it catches up with a similar representation the next day (HU) when it has strengthened to hurricane status. At the HU stage on September 18, 19 and 20th, the model shows a low SLP anomaly and a well closed cyclonic wind circulation at the surface. The simulation successfully replicates the evolution of Hurricane Karl, with some variations in the early stages compared to the reanalysis but a strong resemblance as the hurricane intensifies.

In the lower troposphere

Figure 14 illustrates the horizontal sections of daily relative vorticity and horizontal wind anomalies at 925 hPa from September 15 to 20th, 2004.

On the eve of the system's development, the relative

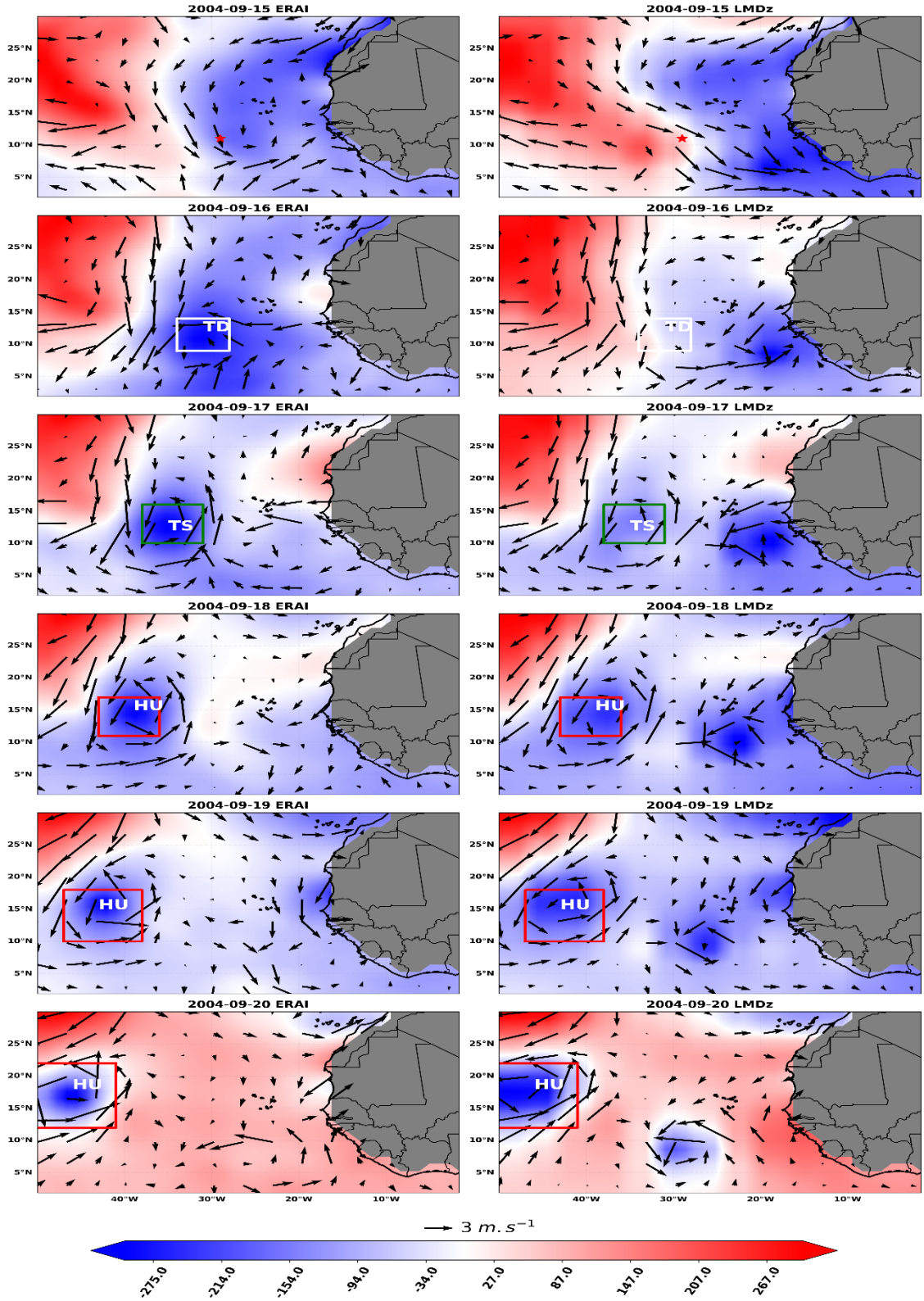

Figure 13. Horizontal cross-sections of daily SLP anomalies (hPa, in colour) and horizontal 10 m wind anomalies (m. s^{-1}, in vectors) of ERAI and LMDZ from 15th to 20th September 2004. The red star represents Karl's birthplace. The white, green and red rectangles represent the system at the stage of Tropical Depression (TD), Tropical Storm (TS) and Hurricane (HU), respectively.

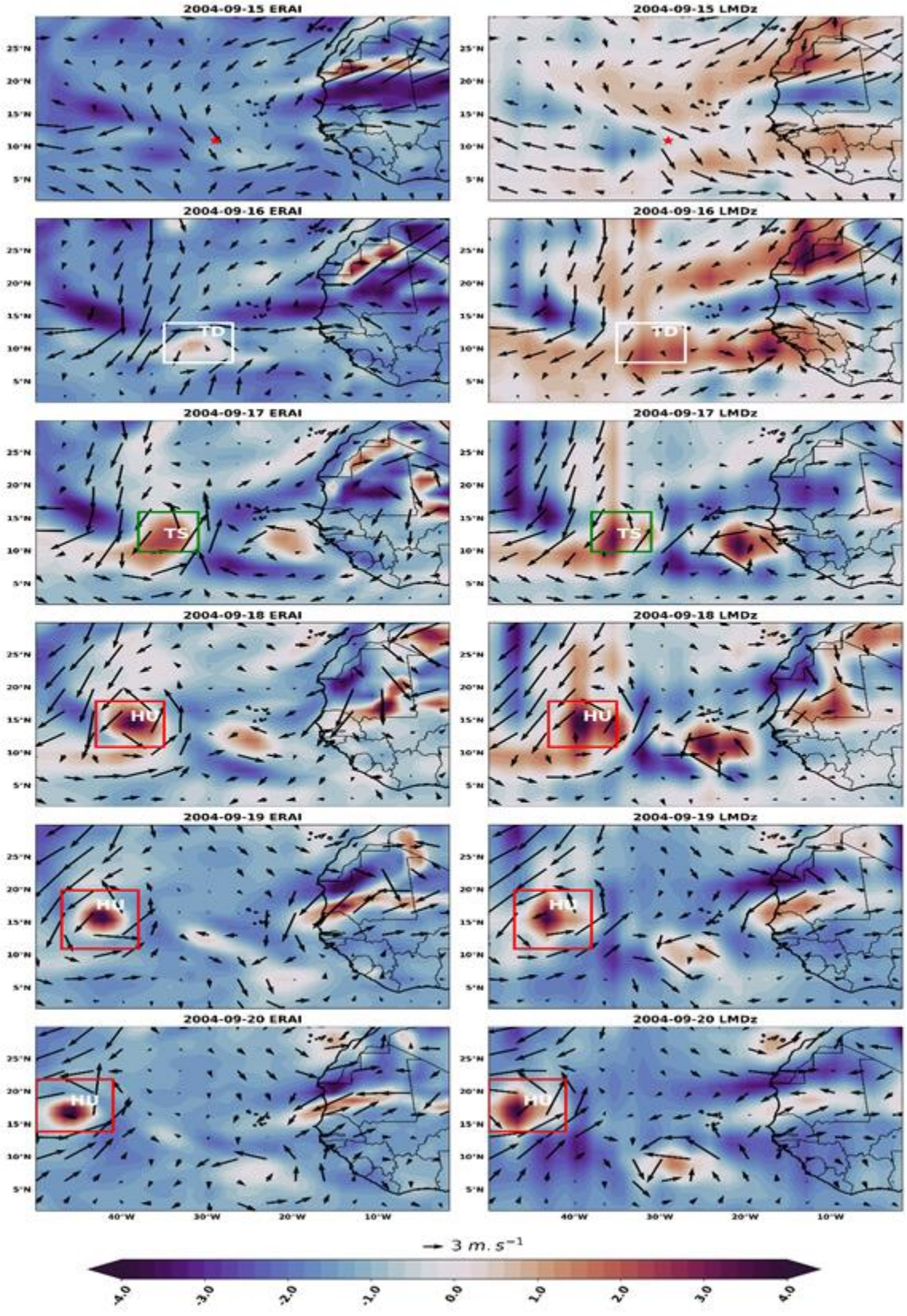

Figure 14. Horizontal cross-sections of daily relative vorticity anomalies (10^{-5} s^{-1}, in colour) and horizontal wind (m. s^{-1}, in vectors) at 925 hPa analysed by ERAI and LMDZ from 15 to 20th September 2004.

vorticity anomaly field in ERAI is negative over most of the basin but shows strengthening southerly winds. This latter is a crucial factor for the cyclonic circulation's development. On September 16th (TD), the reanalysed field exhibits a well-developed cyclonic circulation with a positive vorticity anomaly around 10°N to 30°W. The circulation winds around the system gradually intensify, and becoming more increasingly important during the TS stage (Figure 14TS). The system strengthens into a hurricane on September 18th as it moves north-westward (Figure 14HU) with more representative dynamic structure fields throughout its HU stage. In the model, a positive vorticity anomaly is observed one day before the system's genesis, but the wind anomaly is less structured compared to ERAI on the day of the depression's birth (TD). The delay observed in detecting the TD stage at the surface is not visible at 925 hPa relative vorticity in the model. From the tropical storm (TS) stage onwards, the model successfully replicates the dynamic structures of the system similar to ERAI, although it slightly overestimates the relative vorticity. As the system strengthens into a hurricane on September 18th (HU), LMDZ reproduces it similarly to ERAI. These results indicate that LMDZ provides a reasonable representation of the relative vorticity and dynamic structures of Hurricane Karl, although there are some differences in the early stages of the system's development.

In the mid-troposphere

Figure 15 presents the horizontal sections of daily relative humidity and horizontal wind anomalies at 700 hPa from September 15 to 20th, 2004.

On September 15th, the daily relative humidity anomaly is around 6%(⋆), and it becomes increasingly wet on September 16th (TD) and 17th (TS) with a more pronounced structure. The horizontal wind vortex circulation progressively sets up during these two days in the TD and TS phase. During the intensification into hurricane (HU), the reanalysis shows a system evolving towards the northwest with well-developed winds. The latter bring more moisture and sustain the cyclonic circulation confirming Beven (2004) to the intensification of the disturbance to category 4. LMDZ exhibits a negative daily relative humidity anomaly at the system's birthplace (⋆). However, on the genesis day (TD), the daily relative humidity anomaly becomes positive in the simulation. At 700 hPa, LMDZ struggles to reproduce the system in the TD and TS phases, as previously observed at the surface. On September 18th, when the system strengthens into a hurricane (HU), an intense eddy circulation becomes more evident. From this point onward, similar to ERAI, LMDZ reproduces the daily relative humidity and wind anomalies with a more structured system. The results suggest that LMDZ has difficulty in capturing the early stages of the system's development, particularly in the TD and TS phases.

However, it gradually improves its representation of the system, aligning more closely with ERAI as the system intensifies into a hurricane.

In the upper troposphere

Figure 16 presents the horizontal sections of divergence and horizontal wind anomalies at the 200 hPa level, analyzed by ERAI and simulated by LMDZ from September 15 to 20th, 2004.

On the system's genesis day, ERAI exhibits a divergence intensifying at (10°N to 33°W) with an increasingly significant anticyclonic circulation (TD). On September 17th, when the system strengthens into a tropical storm (TS), ERAI shows a larger divergence anomaly at 200 hPa, which supports deep convection by strengthening the updrafts. As the system evolves into a hurricane (HU), the reanalysis indicates a more substantial divergence anomaly and an anticyclonic circulation. In contrast to ERAI, the simulated divergence anomaly on September 15th remains negative at Karl's genesis location (11°N, 33°W). The model struggles to represent systems with less developed intensity in all layers above. In contrast to ERAI, the simulated divergence anomaly on September 15th remains negative at Karl's genesis location (11°N, 33°W). The model struggles to represent systems with less developed intensity in all layers above. As the system strengthens into a tropical storm (TS) and then into a hurricane (HU), LMDZ provides a more representative simulation, but the divergence anomaly remains less pronounced than in the reanalysis. The results suggest that LMDZ is still unable to capture the early stages of the system's development and has difficulty representing the divergence anomalies seen in ERAI. While it gradually improves its representation of the system as it intensifies, the model's divergence anomalies are generally weaker than those observed in the reanalysis.

The second part of the results, which focuses on synoptic scales, provides insights into the LMDZ climate model's ability to replicate meteorological parameters associated with tropical disturbances. The model demonstrates success in terms of temporal and spatial analysis, as well as tracking a trajectory that is closely aligned with the ERAI reanalysis. These findings indicate that the LMDZ model can effectively reproduce cyclonic structures both in terms of timing and spatial distribution. However, a notable observation from this analysis is the model's delay in detecting the Tropical Depression (TD) stage, which is the initial phase of tropical cyclone development. This suggests that the model may have limitations in representing the early stages of tropical cyclone formation.

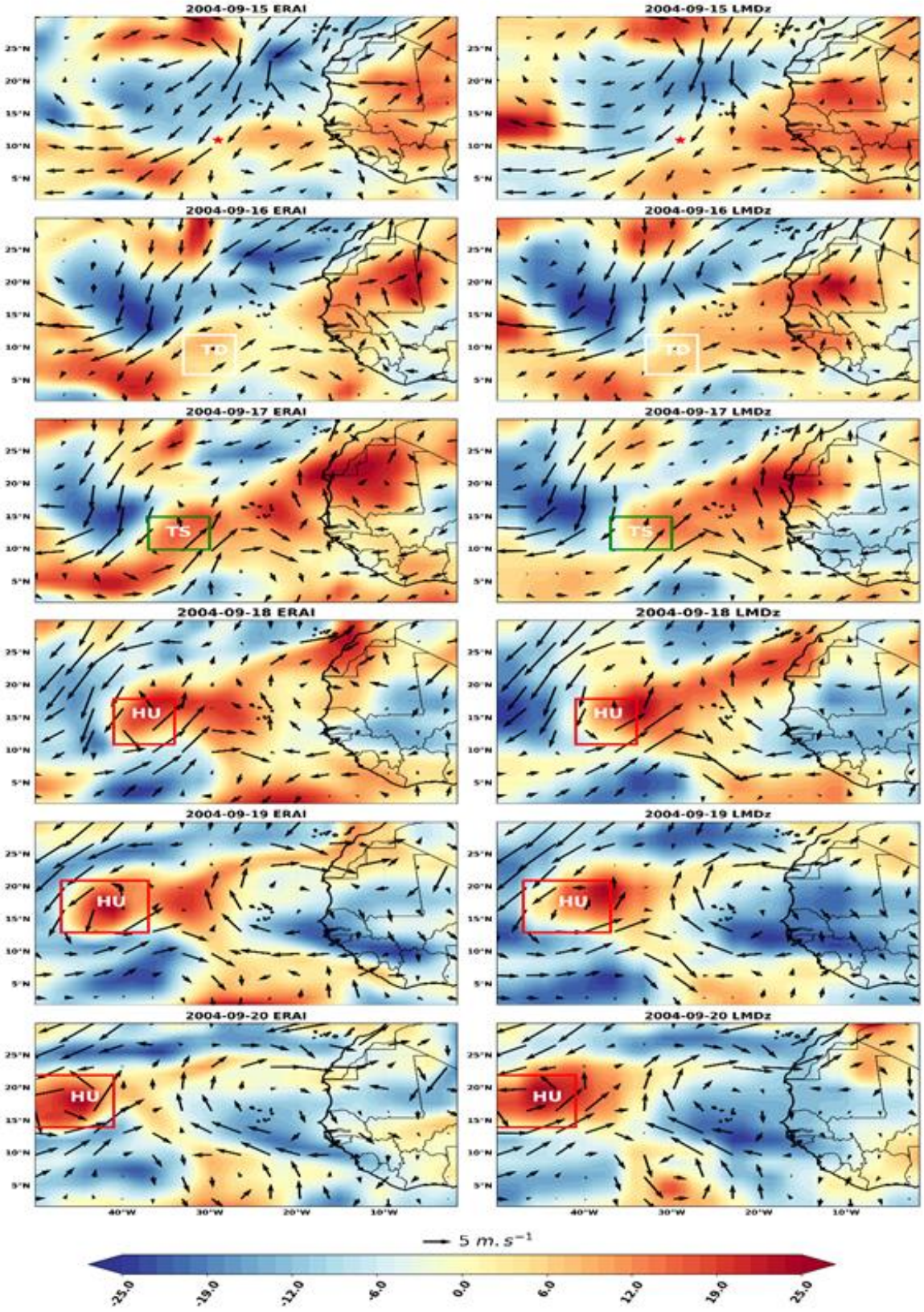

Figure 15. Horizontal cross-sections of daily anomalies of relative humidity (%, in colour) and horizontal wind (m. s^{-1}, in vectors) at 700 hPa analysed by ERAI and LMDZ from 15 to 20th September 2004.

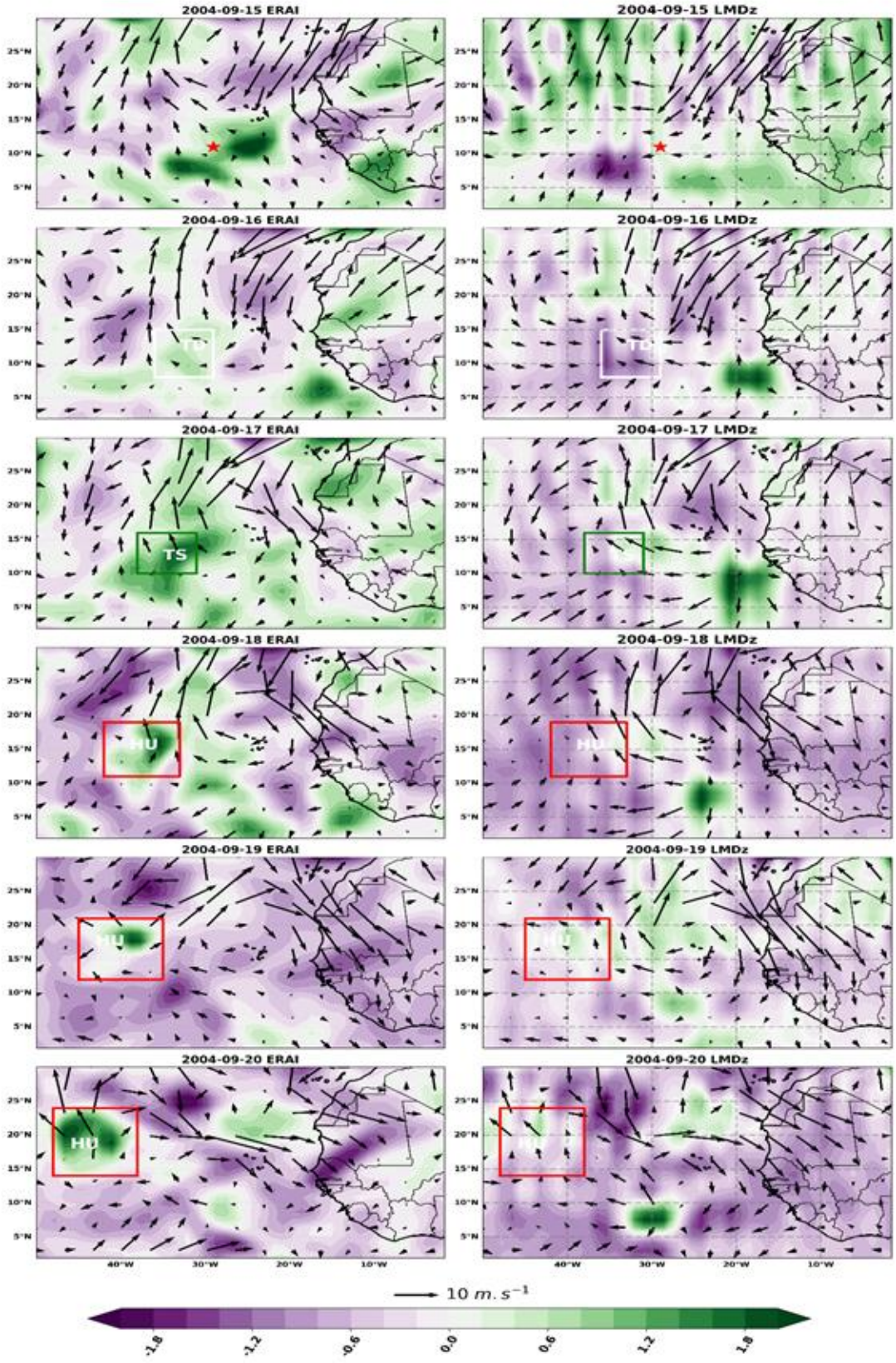

Figure 16. Horizontal cross-sections of daily divergence (10^{-5} s^{-1}, in colour) and horizontal wind (m. s^{-1}, in vectors) anomalies at 200 hPa analysed by ERAI and LMDZ from 15 to 20th September 2004.

CONCLUSION AND PERSPECTIVES

This study aimed to assess the LMDZ model's ability to reproduce cyclogenesis processes and the associated environmental conditions through both interannual and synoptic analyses in the tropical Atlantic region.

The first part of this research was devoted to studying the interannual variability of cyclonic activity in the tropical Atlantic. The study identified two distinct periods of cyclonic activity, characterized by years of high and low cyclonic activity. It revealed an interaction between cyclonic activity and the characteristics of the monsoon, and the model was found to reproduce the monsoon characteristics quite accurately. However, results are more accurate at the surface than in the upper troposphere, quantitatively proven by mean absolute errors being less important from the surface to the high troposphere.

The second part of this work focused on the ability of the LMDZ model to reproduce the determining parameters of the synoptic scale. The model demonstrated a fairly accurate reproduction of the trajectory and intensity distribution of Hurricane Karl in the tropical Atlantic, from its genesis to dissipation. It showed good performance in simulating various parameters in the lower, middle, and upper troposphere. On the other hand, the model was noted to have limitations in capturing the genesis phase of tropical disturbances, indicating potential areas for improvement. It also exhibited a faster translation speed compared to ERAI.

The study provides valuable insights into the LMDZ model's capabilities in simulating cyclonic activity and underlines its potential for further refinement and application in the field of tropical cyclone research. In the led-up to further assess and enhance the model's performance, those results can be improved by expanding the number of cases studied to improve robustness. Also, it would be very interesting to further investigate dynamic and thermodynamic parameters of the ocean in the Main Development Region (MDR) where cyclonic activity has a significant impact. Further refinement and improvement of the model's parametrizations in capturing the genesis stage of tropical cyclones could be an area for future development and research.

CONFLICT OF INTERESTS

The authors have not declared any conflict of interests.

ACKNOWLEDGEMENTS

The authors thank Frederic Hourdin (LMD/CNRS, France) for providing LMDZ simulations, the ANR project ACASIS and the JEAI IRD program through JEAI-CLISAS (Jeune Equipa Associée à l'IRD-Climat et Santé au Sénégal) for funding this research.

REFERENCES

Baek S, Boucher O, Dassas K, Escribano J, Fita L, Forget F, Gainusa-Bogdan A, Guez L, Hourdin C, Hourdin F, Idelkadi A, Lefebvre MP, Li L, Lott F, Madeleine JB, Millour E, Risi C, Sadourny R, Van Phu L (2014). LMDZ5: A documentation, Laboratoire de Meteorologie Dynamique (LMD) 118 p.

Beven J (2004). Tropical Cyclone Report Hurricane Karl 16-24 September 2004. Technical report. National Hurricane Center, Miami USA 9 p.

Burpee RW (1972). The origin and structure of easterly waves in the lower troposphere of North Africa. Journal of the Atmospheric Sciences 29(1):77-90.

Camara M (2006). Cyclogenèse dans l'Atlantique Nord en relation avec le système de mousson en Afrique de l'Ouest. Thèse de doctorat, Institut National Polytechnique De Grenoble, Grenoble 240 p.

Chauvin F, Royer JF, Déqué M (2006). Response of hurricane-type vortices to global warming as simulated by ARPEGE-Climat at high resolution. Climate Dynamics 27:377-399.

Chen TC (2006). Characteristics of African Easterly Waves Depicted by ECMWF Reanalyses for 19912000. Monthly Weather Review 134(12):3539-3566.

Dee DP, Kallen E, Simmons AJ, Haimberger L (2011). Comments on 'Reanalyses suitable for characterizing long-term trends' Bulletin of the American Meteorological Society 92:65-72.

DeMaria M, Knaff JA, Connell BH (2001). A tropical cyclone genesis parameter for the tropical Atlantic. Weather and Forecasting 16(2).

Diallo FB (2012). Rôles des processus couplés convection/surface sur les bilans énergétiques en Afrique de l'ouest. Rapport de stage de 2eme année du Master de dynamique des fluides. Laboratoire de Météorologie dynamique.

Diedhiou A, Janicot S, Viltard A, De Felice P, Laurent H (1999). Easterly wave regimes and associated convection over West Africa and tropical Atlantic: results from the NCEP/NCAR and ECMWF reanalyses. Climate Dynamics 15(11):795-822.

Diedhiou A, Janicot S, Viltard A, De Felice P (2001). Composite patterns of easterly disturbances over West Africa and the tropical Atlantic: A climatology from the 1979–95 NCEP/NCAR reanalyses. Climate Dynamics 18(3):241-253.

Dieng AL (2015). Etude de la cyclogenèse au large des côtes ouest africaines aux échelles synoptiques et saisonnières. Thèse de Doctorat, Ecole Supérieure Polytechnique de Dakar, 151 p.

Fink AH, Reiner A (2003). Spatiotemporal variability of the relation between African Easterly Waves and West African Squall Lines in 1998 and 1999. Journal of Geophysical Research: Atmospheres 108(D11):4332.

Goldenberg SB, CW Landsea, AM Mestas-Nunez, WM Gray (2001). The recent increase of Atlantic hurricane activity: Causes and implications. Science 293:474-479.

Hourdin F, Musat I, Bony S, Braconnot P, Codron F, Dufresne JL, Fairhead L, Filiberti MA, Friedling-stein P, Grandpeix JY, Krinner G, LeVan P, Li ZX, Lott F (2006). The lmdz4 general circulation model: climate performance and sensitivity to parametrized physics with emphasis on tropical convection. Climate Dynamics 27(7-8):787-813.

Jenkins GS, Brito E, Soares E, Chiao S, Lima JP, Tavares B, Monteiro M (2017). Hurricane Fred (2015). Cape Verde's First Hurricane in Modern Times: Observations, Impacts, and Lessons Learned. Bulletin of the American Meteorological Society 98:2603-2618.

Landsea CW (1993). A Climatology of Intense (or Major) Atlantic Hurricanes. Monthly Weather Review 121(6):1703-1713.

Lorck J (2019). Dorian: comment la stagnation aggrave les dégats des ouragans. Monthly Weather Review P 10.

Ohfuchi W, Nkamura H, Yoshioka M, Enomoto T, Takaya K (2004). 10-km mesh meso-scale resolving global simulations of the atmosphere

on the Earth Simulator — Preliminary outcomes of AFES (AGCM for the Earth Simulator). Journal of Earth Simulation 1:8-34.
Oouchi K, Yoshimura J, Ypshimura H, Mizuta R (2006). Tropical cyclone climatology in a global-warming climate as simulated in a 20 km-mesh global atmospheric model: frequency and wind intensity analysis. Journal of the Meteorological Society of Japan 84:259-276.
Pohl B (2017). La modelisation numerique du climat, Centre de Recherches de Climatologie, Biogeosciences, CNRS / UBFC 147p.
Pytharoulis I, Thorncroft C (1999). The low-level structure of African easterly waves in 1995. Monthly Weather Review 127(10):2266-2280.
Rio C, Hourdin F (2008). A thermal plume model for the convective boundary layer: Representation of cumulus clouds. Journal of the Atmospheric Sciences 65:407-425.
Rio C, Hourdin F, Grandpeix JY, Lafore JP (2009). Shifting the diurnal cycle of parameterized deep convection over land. Geophysical Research Letters 36:L07809.
Sall SM, Sauvageot H (2005). Cyclogenesis off the African Coast: The Case of Cindy in August 1999. Monthly Weather Review 133(9):2803-2813.
Sane Y (2011). Représentation du cycle de vie des systems convectifs dans le modèle LMDz pendant la campagne AMMA 2006. Thèse de doctorat, Université Pierre et Marie Curie 206 p.
Senghor H, Machu É, Hourdin F, and Gaye AT (2017). Seasonal cycle of desert aerosols in western Africa: analysis of the coastal transition with passive and active sensors. Atmospheric Chemistry and Physics 17:8395-8410.
Shen BW, R Atlas, JD Chern, O Reale, SJ Lin (2006). The 0.125 degree finite-volume general circulation model on the NASA Columbia supercomputer: Preliminary simulations of mesoscale vortices. Geophysical Research Letters 33(5).
Weinkle J, Landsea C, Collins D, Musulin R, Crompton RP, Klotzbach PJ, Pielke R (2018). Normalized hurricane damage in the continental United States 1900-2017. Nature Sustainability 1:808-813.

Vol. 17(11), pp. 294-301, November 2023
DOI: 10.5897/AJEST2023.3218
Article Number: 20E413B71538
ISSN: 1996-0786
Copyright ©2023
Author(s) retain the copyright of this article
http://www.academicjournals.org/AJEST

ACADEMIC JOURNALS
expand your knowledge

African Journal of Environmental Science and Technology

Full Length Research Paper

The application of composting materials to degrade polycyclic aromatic hydrocarbon on oil field drill cuttings

Mary Allagoa

Environmental Soil Science, King's College, University of Aberdeen, Aberdeen, AB24 3FX, Scotland, United Kingdom.

Received 9 August, 2023; Accepted 20 November, 2023

The potential effects of using poultry droppings and mushroom substrate, either alone or in combination, as amendments or nutrient supplements for hydrocarbon biodegradation were investigated in this study. The rates of biodegradation of drill cuttings were studied over remediation periods of 4 and 8 weeks under laboratory conditions. The concentrations of polycyclic aromatic hydrocarbons (PAHs) in untreated drill cuttings, spent mushroom substrate, and poultry manure were 18.464, 13.29, and 19.59 mg kg^{-1}, respectively. The first-order empirical model was employed to predict changes in hydrocarbon concentrations. Subsequently, Biodegradation Efficiency (BDE), Diagnostic Ratio, and Toxicity Equivalent Factor (TEF) were determined. Analysis of the empirical data revealed a highly statistically significant difference in PAHs at 8 weeks due to the amendment. Notably, spent mushroom substrate (SMS) exhibited better performance on its own compared to animal waste (poultry droppings). However, a combination of poultry droppings and SMS (4:1:1) resulted in higher values of BDE. Diagnostic ratios calculated indicated that PAHs originated from both combustion and anthropogenic sources. TEF demonstrated a reduction in value from 4 to 8 weeks, with the 14 individual PAHs investigated showing a 50% reduction in fluoranthene. Conversely, the biodegradation rate constants obtained were higher with lower half-life times for the various amendments using plant and animal-source organic wastes, either alone or in combinations.

Key words: Toxicity equivalent factor (TEF), biodegradation efficiency (BDE), diagnostic ratio, polycyclic aromatic hydrocarbons (PAHs), drill cuttings, poultry droppings, spent mushroom substrate.

INTRODUCTION

A substantial volume of oily sludge is generated during oil production and processing activities, with oil and gas drilling operations worldwide producing drill-cutting wastes. Managing fossil fuel waste has become a prominent topic in the environmental industry in recent years. Historically, these drill cuttings were often disposed of in water bodies or on land without any prior treatment (Browning and Seaton, 2005). Additionally, companies

E-mail: maryallagoa@gmail.com.

Author(s) agree that this article remain permanently open access under the terms of the Creative Commons Attribution License 4.0 International License

engaged in burning fossil fuels commonly stockpiled waste, either relocating it or burying the drill cuttings, thereby exacerbating contamination risks.

Most fossil fuel waste, specifically drill cuttings, contains a considerable amount of polycyclic aromatic hydrocarbons (PAHs), which serve as a potent energy source for mycelium (spent mushroom compost). Drill cuttings have been characterized by a relatively high content of PAHs (DPR, 2002) and heavy metals (Khajiagbe et al., 2014). Over the years, various methods, including thermal treatment technologies, solidification/stabilization (Shaffer et al., 1998; Allagoa, 2014), and mechanochemistry (Peng et al., 2018), have been employed for the management of drill cuttings.

Since the 1970s, biological treatments have been actively utilized for hydrocarbon degradation and are now considered among the most effective cleanup alternatives for soil (Kuppusamy et al., 2017). Composting, as an *ex-situ* bioremediation technology, is particularly adept at treating large volumes of polluted soils. It plays a crucial role in the sustainable recycling of organic waste (Fermor, 1993; Tuomela et al., 2000; Andrew et al., 1999; Hachicha et al., 2009; Greenway and Song, 2002) and results in a marketable end product used as a soil conditioner and organic fertilizer.

The addition of organic waste is essential to promote the development of a diverse microbial community capable of breaking down complex contaminants (Aitken et al., 1992; Jorgensen et al., 2000; Ma et al., 2016). A case study on Mushroom compost-assisted remediation of soil contaminated with PAHs from a manufactured gas plant was conducted in a thermally insulated composting chamber. The degradation of individual PAHs ranged from 20.6% at the end of 54 days of composting, with a subsequent increase in PAH removal to 37-80% after 100 days of maturation (Malachova et al., 2003).

Paladino et al. (2016) conducted a study on the bioremediation of drilling wastes contaminated with heavy hydrocarbons through composting. Following the experiment, a substantial degradation of total hydrocarbons (approximately 82%) and the 16 USEPA-listed PAHs (approximately 93%) was observed.

Kinetic models, known for predicting residual contaminant concentrations, have proven useful in previous studies (Venosa and Holder, 2007; Bayen et al., 2009).

In the present study, compost experiments were conducted on drill cuttings, and subsequently, we calculated the first-order empirical model to predict changes in hydrocarbon concentrations. Finally, we determined Biodegradation Efficiency (BDE), diagnostic ratios, and the toxicity equivalent factor (TEF).

MATERIALS AND METHODS

Study area description

Rivers State produces a significant portion of Nigeria's crude oil. The city is situated within the tropical rainforest zone, experiencing a mean annual rainfall of approximately 2400 mm, a monthly relative humidity of 85%, and mean daily minimum and maximum temperatures of about 25 and 31.5°C, respectively. Table 1 shows the experimental layout.

Laboratory analysis

The samples were air-dried and weighed. A ratio of 1:2 was maintained between the samples and the solvent. Analytical grade hexane and dichloromethane were used in the required quantities for extraction when needed. The dry/cold extraction method was employed for sample separation. Following extraction, the resulting extract was prepared for gas chromatography analysis.

The diagnostic ratios on PAHs to determine their sources

PAH ratios determine PAH sources, clarify samples by locations, and estimate (Yunker et al., 2002). Table 2 shows the diagnostic ratios used in this study with their typical values for particular processes.

Benzo[a]Pyrene equivalent (B[a]Peq) estimation

BaP equivalent concentration (BaPeq) evaluated the toxicities of PAHs in sampling sites. Therefore, the total PAH concentration is expressed as B[a]Peq to illustrate the toxic potency (Igbiri et al., 2017). As proposed earlier by Nisbet and Lagoy (1992) and Igbiri et al. (2017), the B[a]Peq is the summation of the B[a]Peqi. It is the value for specific PAHs or individual PAH concentrations in the sample (cPAHi) multiplied by its toxic equivalency factor (TEFPAHi). Table 3 shows the toxicity equivalent factor value of the individual PAHs.

$$B[a]Peq = \sum(BaPeqi) = \sum(cPAHi \times TEFPAHi) \; or \; \sum BaPeq = \sum Ci \times TEFi \quad (1)$$

where Ci is the concentration of individual PAHs and TEFi is the corresponding toxic equivalency factor.

Quantification and characterization of degradation

The biodegradation rates of PAHs were evaluated by comparing the reaction rate constants of the pseudo-first-order kinetics as described by Okparanma et al. (2011) and expressed as:

$$\boldsymbol{Log\ Co - Ct = Log\ Co - \left(\frac{K1}{2.303}\right) \times t} \quad (2)$$

Make K_1 the subject formula from Okparanma et al. *(*2011).

$$\boldsymbol{K1 = \frac{2.303}{t} \times [(Log\ Co) - (Log\ Co - Ct)]} \quad (3)$$

where K is the apparent constant reaction rate of the pseudo-first-order (1/week) and t is the time (weeks).

Then, the half-life of the respective PAHs:

$$T_{1/2} = 0.693 / K_1 \quad (3)$$

Biodegradation efficiency (BDE):

$$\boldsymbol{BDE(\%) = \frac{Co - Ct}{Co} \times 100} \quad (4)$$

Table 1. Experimental layout.

Reactor	Compost
Control	Untreated drill-cuttings
Reactor 1	Drill cuttings + top soil + (PD+SD) that is, 4:1:1; 2000 g + 500 g + 500 g
Reactor 2	Drill cuttings + top soil + SMS that is, 4:1:1; 2000 g + 500 g + 500 g
Reactor 3	Drill cuttings + top soil + (PD+SD) that is, 4:1:2; 2000 g + 500 g + 1000 g
Reactor 4	Drill cuttings + top soil + SMS that is, 4:1:2; 2000 g + 500 g + 1000 g
Reactor 5	Drill cuttings + top soil + (PD+SD) that is, 4:1:4; 2000 g + 500 g + 2000 g
Reactor 6	Drill cuttings + top soil + SMS that is, 4:1:4; 2000 g + 500 g + 2000 g
Reactor 7	Drill cuttings + top soil + (PD+SD) + SMS that is, 4:1:1; 2000 g + 500 g + 500 g

PD - Poultry droppings, SD - saw dust, SMS - spent mushroom substrate.

Table 2. Diagnostic ratios used in this study with their typical values for particular processes.

PAHs ratio	Values	Source	References
∑LMW/∑HMW	<1	Pyrogenic/Anthropogenic	Zhang et al. (2008)
	>1	Petrogenic/Natural	
Ant/(ant + Phe)	<0.1	Petrogenic/Natural	Pies et al. (2008)
	>0.1	Pyrogenic/Anthropogenic	
BaA/(BaA + CHR)	<0.2	Petrogenic/Natural	Yunker et al. (2002)
	0.35	Combustion	

Table 3. Toxicity equivalent factor value of the individual PAHs.

PAHs	Toxicity equivalent factor	Reference
Naphthalene	0.001	Nisbet and Lagoy (1992)
Phenanthrene	0.001	
Anthracene	0.01	
Acenaphthelene	0.001	
Acenaphthylene	0.001	
Flourene	0.001	
Pyrene	0.001	
Chrysene	0.01	
Benzo[a]anthracene	0.1	
Fluoranthane	0.001	

where C_o is the initial concentration and C_t is the final concentration.

Statistical analysis

The data were presented as the mean of triplicates (n=3) ± standard error. ANOVA or general linear model (GLM) tests and t-test in MINITAB 16.0 were identified as $p \leq 0.05$.

RESULTS AND DISCUSSION

The mean concentrations of PAHs in the drill cuttings with amended plant residues and animals, either alone or in combination, are presented in Table 4. It was observed that the percentage reduction of PAHs was rapid at 8 weeks in the amended wastes. By the end of 8 weeks, the ∑PAHs reduction in the seven reactors is as follows: 31.85, 53.77, 44.83, 62.32, 59.27, 58.96, and 52.87%. At the conclusion of the remediation period (8 weeks), reactor 2 with SMS (4:1:2) exhibited the highest reduction in PAHs concentration (65.06%) (Figure 1). This was followed relatively by reactor 4 (56.82%), reactor 6 (53.62%), reactor 4 (50.24%), reactor 5 (48.32%), reactor 3 (45.93%), and reactor 1 (28.55%).

Adesodun and Mbagwu (2008) confirmed in their study that poultry droppings performed better at high oil

Table 4. 14PAHs concentration on the seven reactors for 4 and 8 weeks.

PAHs	PD + SD (4:1:1)		SMS (4:1:1)		PD + SD (4:1:2)		SMS (4:1:2)		PD +SD (4:1:4)		SMS (4:1:4)		(PD+SD) + SMS (4:1:1)	
	4weeks	8weeks	4weeks	8weeks	4weeks	8weeks	4weeks	8weeks	4weeks	8weeks	4weeks	8weeks	4weeks	8weeks
1	49.8	44.0	2.1	1.3	31.7	22.0	11.3	3.3	8.0	2.4	5.1	1.3	4.0	1.1
2	39.9	30.0	3.2	1.3	11.9	7.4	12.9	2.4	24.8	7.6	3.5	2.4	16.2	9.6
3	753.9	545.9	173.4	70.5	337.5	92.2	176.3	51.6	162.1	38.4	76.6	31.6	154.7	59.0
4	814.8	617.2	445.9	356.3	725.2	565.9	356.2	139.6	286.7	58.9	154.9	32.2	263.0	137.5
5	2457.6	2110.8	2064.6	673.9	743.2	605.7	956.9	429.3	515.6	296.3	210.6	157.2	505.3	301.5
6	2157.2	1856.2	1051.0	228.5	1679.1	1072.1	1248.7	663.2	305.2	147.6	455.3	256.8	1128.7	577.7
7	2464.0	1924.3	1936.1	1219.3	2224.7	1103.6	875.7	158.2	634.4	229.9	537.3	339.7	917.2	839.6
8	1134.9	1009.1	405.0	300.6	1031.1	451.0	1030.8	747.6	433.7	289.8	143.5	39.2	1034.2	447.9
9	1300.1	182.5	871.3	217.0	1477.3	850.0	1075.0	667.6	513.0	262.8	158.3	36.6	595.7	340.2
10	238.8	191.0	80.5	50.9	1128.5	47.1	468.7	227.7	271.9	25.2	64.9	19.8	346.0	227.7
11	127.2	64.9	615.1	57.6	404.3	100.5	188.2	47.7	250.9	94.5	444.5	225.3	453.7	50.7
12	66.5	47.3	157.1	132.6	183.3	103.8	215.7	52.3	162.2	111.1	132.8	31.4	240.6	25.0
13	218.8	99.4	521.9	195.8	660.7	516.3	769.6	192.3	659.9	118.7	463.9	80.3	135.1	61.4
14	924.1	385.4	2868.4	406.5	1008.2	759.3	3511.3	1321.7	1884.9	1358.8	1415.3	724.9	1749.0	819.7
Total	12747.4	9108.0	11195.5	3912.0	11646.5	6296.8	10897.2	4704.5	6113.0	3041.7	4266.4	1978.7	7543.2	3898.6

1- Naphthalene, 2- Acenaphthylene, 3- Acenaphthelene, 4- Flourene, 5- Phenanthrene, 6- Anthracene, 7- Fluoranthene, 8- Benzo[a]anthracene, 9- Chrysene, 10- Benzo[b]Fluoranthene, 11- Benzo[a]pyrene, 12- Indeno [1,2,3-cd]pyrene, 13- Dibenzo[a,h]anthracene, 14- Indeno[1,2,3-cd]pyrene.

pollution levels, while Phan and Sabaratnam (2012) showed that spent mushroom substrate was more effective at both low and high oil pollution levels. According to Juhasz and Naidu (2000), many bacteria rapidly transform low molecular weight PAHs. Shuttleworth and Cerniglia (1995), as well as Kanaly and Harayama (2000), confirmed that high molecular weight PAHs are more recalcitrant in the environment and may resist both chemical and microbial degradation. Analyzing the data from Table 5 on reactors 2, 4, and 6, it was observed that Acenaphthene (62.95%) degraded better than all the other 3-ringed compounds. Chrysene (63.28%) demonstrated superior degradation as compared to all 4-ringed compounds, while Dibenzo[a.h]anthracene (73.39%) degraded better than all the 5-ringed compounds investigated in this study. Boyle et al. (1992) and Song (1999) found greater disappearance rates after inoculating their samples with white rot fungi. During this investigation, Spent Mushroom Substrate (SMS) demonstrated the ability to degrade a significant amount of 3, 4, 5, and 6-ringed PAHs, highlighting its potential for PAH degradation. Analyzing the data from the table for reactors 1, 3, and 5, it was observed that Acenaphthene (58.87%) degraded more effectively than all the other 3-ringed compounds. Chrysene (59.06%) demonstrated superior degradation compared to all 4-ringed compounds, while Benzo[b]Fluoranthane (68.85%) degraded better than all the 5-ringed compounds investigated in this study. Poultry droppings were reported to enhance the degradation of hydrocarbons in soil compost mixtures (Agarry et al., 2010). The increase in microbial population and rapid degradation of some of the PAHs continued with an increase in amendments to the drill cuttings with poultry droppings. In Table 5, a 31.85 to 59.27% reduction was observed after additional amendment at 8 weeks. Analyzing the data from Table 5, reactor 7 was observed to have Acenaphthene (61.8%) degraded more effectively than all the other 3-ringed compounds. Benzo[a]anthracene (56.7%) demonstrated superior degradation compared to all 4-ringed compounds, while Benzo[a]pyrene (88.8%) and Indeno[1,2,3-cd] pyrene (89.6%) degraded better than all the 5-ringed compounds investigated. Since poultry manure is rich in carbon and mineral

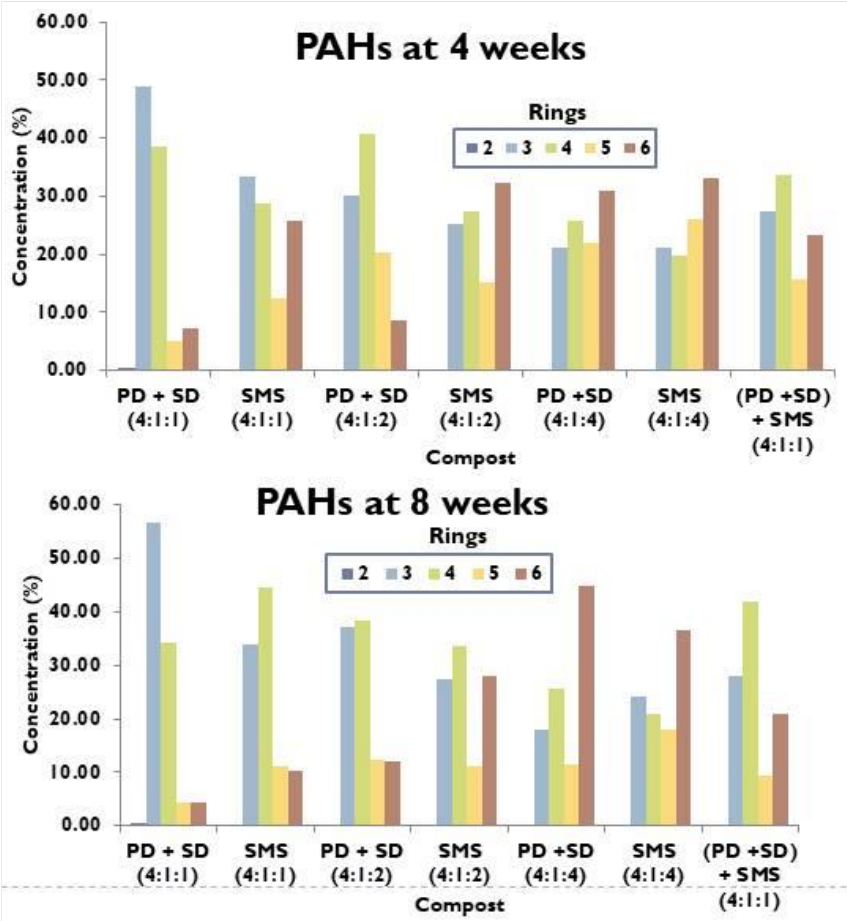

Figure 1. PAHs at 4 and 8 weeks.

Table 5. BDE (%) of the individual PAHs investigated.

PAHs	BDE (%)						
	PD + SD (4:1:1)	SMS (4:1:1)	PD + SD (4:1:2)	SMS (4:1:2)	PD +SD (4:1:4)	SMS (4:1:4)	(PD+SD) + SMS (4:1:1)
1	11.6	39.7	30.6	71.0	70.1	74.5	72.4
2	24.7	58.8	37.8	81.3	69.4	31.2	40.7
3	27.6	59.3	72.7	70.7	76.3	58.8	61.8
4	24.3	20.1	22.0	60.8	79.5	79.2	47.7
5	14.1	67.4	18.5	55.1	42.5	25.4	40.3
6	14.0	78.3	36.1	46.9	51.6	43.6	48.8
7	21.9	37.0	50.4	81.9	63.8	36.8	8.5
8	11.1	25.8	56.3	27.5	33.2	72.6	56.7
9	86.0	75.1	42.5	37.9	48.8	76.9	42.9
10	20.0	36.8	95.8	51.4	90.7	69.5	34.2
11	48.9	90.6	75.1	74.6	62.3	49.3	88.8
12	28.8	15.6	43.4	75.8	31.5	76.3	89.6
13	54.6	62.5	21.9	75.0	82.0	82.7	54.6
14	58.3	85.8	24.7	62.4	27.9	48.8	53.1

1- Naphthalene, 2- Acenaphthylene, 3- Acenaphthelene, 4-Flourene, 5- Phenanthrene, 6- Anthracene, 7- Fluoranthene, 8-Benzo[a]anthracene, 9-Chrysene, 10-Benzo[b]Fluoranthene, 11-Benzo[a]pyrene, 12- Indeno[1,2,3-cd]pyrene, 13-Dibenzo[a,h]anthracene, 14- Indeno[1,2,3-cd]pyrene.

Table 6. Three Diagnosti ratio calculated for 4 and 8 weeks.

Compost	4 weeks			8 weeks		
	∑LMW/∑HMW	Ant/(ant + Phe)	BaA/(BaA + CHR)	∑LMW/∑HMW	Ant/(ant + Phe)	BaA/(BaA + CHR)
PD + SD (4:1:1)	1.0	0.5	0.5	1.3	0.5	0.8
SMS (4:1:1)	0.5	0.3	0.3	0.5	0.3	0.6
PD + SD (4:1:2)	0.4	0.7	0.4	0.6	0.6	0.3
SMS (4:1:2)	0.3	0.6	0.5	0.4	0.6	0.5
PD +SD (4:1:4)	0.3	0.4	0.5	0.2	0.3	0.5
SMS (4:1:4)	0.3	0.7	0.5	0.3	0.6	0.5
(PD +SD) + SMS (4:1:1)	0.4	0.7	0.6	0.4	0.7	0.6

Table 7. The TEF of the seven reactors in 4 and 8 weeks for the 10PAHs.

PAHs	PD + SD (4:1:1)		SMS (4:1:1)		PD + SD (4:1:2)		SMS (4:1:2)		PD +SD (4:1:4)		SMS (4:1:4)		(PD+SD) + SMS (4:1:1)	
	4 weeks	8 weeks	4 weeks	8 weeks	4 weeks	8 weeks	4 weeks	8 weeks	4 weeks	8 weeks	4 weeks	8 weeks	4 weeks	8 weeks
1	0.05	0.04	0.002	0.001	0.03	0.02	0.01	0.003	0.01	0.002	0.005	0.001	0.004	0.001
2	2.46	2.11	2.065	0.674	0.74	0.61	0.96	0.429	0.52	0.296	0.211	0.157	0.505	0.302
3	21.57	18.56	10.510	2.285	16.79	10.72	12.49	6.632	3.05	1.476	4.553	2.568	11.287	5.777
4	0.75	0.55	0.173	0.071	0.34	0.09	0.18	0.052	0.16	0.038	0.077	0.032	0.155	0.059
5	0.04	0.03	0.003	0.001	0.01	0.01	0.01	0.002	0.02	0.008	0.004	0.002	0.016	0.010
6	0.81	0.62	0.446	0.356	0.73	0.57	0.36	0.140	0.29	0.059	0.155	0.032	0.263	0.138
7	13.00	1.83	8.713	2.170	14.77	8.50	10.75	6.676	5.13	2.628	1.583	0.366	5.957	3.402
8	113.49	100.91	40.498	30.063	103.11	45.10	103.08	74.756	43.37	28.979	15.828	3.663	59.567	34.017
9	2.46	1.92	1.936	1.219	2.22	1.10	0.88	0.158	0.63	0.230	0.143	0.039	1.034	0.448
10	127.16	64.92	615.100	57.640	404.26	100.48	188.15	47.730	250.91	94.470	444.460	225.310	453.660	50.740

1- Naphthalene, 2- Phenanthrene, 3– Anthracene, 4- Acenaphthylene, 5- Acenaphthelene, 6- Flourene, 7- Pyrene , 8- Chrysene, 9- Benzo[a]anthracene, 10- Fluoranthene.

nutrients, particularly nitrogen (Chan et al., 2008; Atagana, 2004), and SMS has the ability to degrade lignin and PAHs, a combination of poultry droppings and SMS degraded the PAHs better in the drill cuttings than with either amendment alone.

The higher the biodegradation rate constants, the faster the rate of biodegradation, and consequently, the lower the half-life times. It can be observed from Table 6 that among the reactors amended with poultry droppings (PD) + spent mushroom substrate (SD) and SMS, or with a combination of both amendments, reactor 6 exhibited a higher biodegradation rate constant (k) of 0.8073 week^{-1} and a lower half-life time (T1/2 = 0.86 weeks, R^2 = 0.135) for Acenaphthylene compared to other PAHs (Table 6). However, this was relatively followed by reactor 1, which was amended with animal source waste, PD + SD (k = 0.6548 week^{-1} and $T_{1/2}$ = 1.1 weeks, R^2 = 0.133), reactor 3 (k = 0.4455 week^{-1} and $T_{1/2}$ = 1.6 weeks, R^2 = 0.106), reactor 7 (k = 0.3427 week^{-1} and $T_{1/2}$ = 2.02 weeks, R^2 = 0.058), reactor 2 (k = 0.2785 week^{-1} and $T_{1/2}$ = 2.5 weeks, R^2 = 0.029), reactor 5 (k = 0.1551 week^{-1} and $T_{1/2}$ = 4.47 weeks, R^2 = 0.002) and reactor 4 (k = 0.1477 week^{-1} and $T_{1/2}$ = 4.7 weeks, R^2 = 0.066).

PAH ratios were calculated to determine PAH sources, clarify samples by locations, and estimate (Yunker et al., 2002). In Table 7, the calculated

Table 8. The biodegradation rate constant and half of the 14PAHs.

PAHs	PD + SD (4:1:1)		SMS (4:1:1)		PD + SD (4:1:2)		SMS (4:1:2)		PD +SD (4:1:4)		SMS (4:1:4)		(PD+SD) + SMS (4:1:1)	
	K_1	$T_{1/2}$	K_1	$T_{1/2}$	K_1	$T_{1/2}$	K_1	$T_{1/2}$	K_1	$T_{1/2}$	K_1	$T_{1/2}$	K_1	$T_{1/2}$
1	0.655	1.1	0.278	2.5	0.319	2.2	0.148	4.7	0.155	4.5	0.068	10.2	0.033	20.9
2	0.345	2.0	0.144	4.8	0.446	1.6	0.084	8.3	0.118	5.9	0.807	0.9	0.343	2.0
3	0.030	22.9	0.041	16.8	0.018	37.6	0.032	21.9	0.029	23.5	0.077	9.0	0.043	16.2
4	0.033	21.3	0.066	10.6	0.040	17.4	0.023	30.4	0.018	38.7	0.028	24.5	0.039	17.7
5	0.022	31.4	0.005	147.9	0.047	14.9	0.011	60.3	0.026	26.7	0.095	7.3	0.028	24.7
6	0.025	27.7	0.007	104.9	0.011	60.3	0.011	62.4	0.032	21.9	0.028	24.8	0.012	60.0
7	0.014	49.4	0.010	69.9	0.006	110.9	0.007	98.2	0.013	51.5	0.029	23.5	0.087	8.0
8	0.055	12.6	0.055	12.7	0.011	65.8	0.023	29.7	0.039	17.6	0.035	19.7	0.010	66.5
9	0.005	148.7	0.008	84.3	0.011	64.4	0.016	43.4	0.022	31.1	0.030	23.4	0.023	30.4
10	0.110	6.3	0.133	5.2	0.004	194.4	0.023	30.8	0.013	53.0	0.066	10.5	0.046	15.1
11	0.067	10.3	0.007	95.3	0.015	45.7	0.028	25.2	0.029	23.8	0.025	28.0	0.010	71.1
12	0.201	3.4	0.200	3.5	0.058	11.9	0.024	28.6	0.092	7.5	0.034	20.4	0.015	46.4
13	0.039	18.0	0.016	42.8	0.043	16.0	0.009	76.0	0.009	78.5	0.011	60.6	0.056	12.4
14	0.011	62.7	0.002	283.9	0.027	26.0	0.003	211.1	0.014	50.5	0.010	72.6	0.007	96.0

1- Naphthalene, 2- Acenaphthylene, 3- Acenaphthelene, 4- Flourene, 5- Phenanthrene, 6- Anthracene, 7- Fluoranthene, 8- Benzo[a]anthracene, 9- Chrysene, 10- Benzo[b]Fluoranthene, 11- Benzo[a]pyrene, 12- Indeno[1,2,3- cd]pyrene, 13- Dibenzo[a,h]anthracene, 14- Indeno[1,2,3-cd]pyrene.

ratios ∑LMW/∑HMW, Ant/(Ant+Phe), and BaA/(BaA+Chry) were observed to be <1, >0.1, and >0.35, respectively. These values may indicate that PAHs were primarily derived from anthropogenic and combustion sources. The B[a]Peq is the summation of the B[a]Peqi, calculated by multiplying the value for specific PAHs or individual PAH concentrations in the sample (cPAHi) by its toxic equivalency factor (TEFPAHi), as proposed earlier by Nisbet and Lagoy (1992) and Igbiri et al. (2017). TEF estimates the exposure risks modeled by individual and total PAHs to human health. In Table 8, the modeled values for the 10 PAHs indicate the exposure risk of total PAHs to human health at 8 weeks, which reduced to 32.05, 86.10, 69.21, 56.98, 57.85, 50.29, and 82.18% with the amended compost. The results indicate that compost with the specified ratios of plant and animal waste proved effective in reducing PAHs from crude oil waste (drill cuttings). However, the study suggests that extended remediation periods are advisable to maintain PAHs at a more reduced concentration and in an inactive form.

Furthermore, the study concludes that the majority of PAHs found in the environment are primarily a result of human activities, as indicated by the diagnostic ratios calculated. Notably, the half-life of the PAHs was reduced to less than a week for reactor 6, underscoring the significant impact of composting on the investigated PAHs.

Conclusion

The drill cuttings are deemed unsafe for land disposal without prior treatment. The current studies confirm that the use of plant residues and animal dung wastes, whether used alone or in combination, enhances the rate of petroleum hydrocarbon biodegradation in contaminated drill cuttings. In conclusion, a more pronounced effect was observed with the combination of poultry droppings and SMS, demonstrating better degradation of PAHs in the drill cuttings compared to the use of a single amendment.

CONFLICT OF INTERESTS

The author has not declared any conflict of interests.

REFERENCES

Adesodun JK, Mbagwu JSC (2008). Biodegradation of waste-lubricating petroleum oil in a tropical alfisol as mediated by

animal droppings. Bioresource Technology 99(13):5659-5665.
Agarry SE, Owabor CN, Yusuf RO (2010). Bioremediation of Soil Artificially Contaminated with Petroleum Hydrocarbon Oil Mixtures: Evaluation of the Use of Animal Manure and Chemical Fertilizer. Bioremediation Journal 14:189-195.
Allagoa M (2014). "Effective use of Cementitious Materials, Ground Granulated Blast Furnace Slag and Bentonite in treating contaminants on polluted land", Proceedings of the Shale Energy Engineering 2014 conference, held in Pittsburgh, Pennsylvania, July 21-23, 2014. Sponsored by the Energy Division of ASCE.
Andrew SS, Lohr L, Cabrera ML (1999). A bioeconomic decision model comparing composted and fresh litter for winter squash. Agricultural Systems 61(3):165-178.
Aitken MD, Heck PE, Mines RO, Sherrard JH (1992). Activated sludge. Water Environment Research 64(4):347-359.
Atagana HI (2004). Co-composting of PAH-contaminated soil with poultry manure. Letters in Applied Microbiology 39(2):163-168.
Bayen S, ter Laak TL, Buffle J, Hermens JLM (2009). Critical review dynamic exposure of organisms and passive samplers to hydrophobic chemicals. Environmental Science and Technology 43:2206-2215.
Boyle CD, Kropp BR, Reid ID (1992). Solubilization and Mineralization of Lignin by White Rot Fungi. Applied and Environmental Microbiology 58(10):3217-3224.
Browning K, Seaton S (2005). Drilling Waste Management: Case Histories Demonstrate That Effective Drilling Waste Management Can Reduce Overall Well-Construction Costs. SPE Annual Technical Conference and Exhibition, Dallas, Texas, October 2005. Paper Number: SPE-96775-MS.
Chan KY, Van Zwieten L, Meszaros I, Downie A, Joseph S (2008). Using poultry litter biochars as soil amendments. Australian Journal of Soil Research 46(5):437-444.
Department of Petroleum Resources (DPR) (2002). Environmental Guidelines and Standards for the Petroleum Industry in Nigeria (EGASPIN).
Fermor TR (1993). Applied aspects of composting and bioconversion of lignocellulosic materials an overview. International Biodeterioration and Biodegradation 31:87-106.
Greenway GM, Song QJ (2002). Heavy metal speciation in the composting process. Journal of Environmental Monitoring 4(2):300-305.
Hachicha R, Hachicha S, Trabelsi I, Woodward S, Mechichi T (2009). Technical Note Evolution of the fatty fraction during co-composting of olive oil industry wastes with animal manure: Maturity assessment of the end product. Chemosphere 75(10):1382-1386.
Jorgensen KS, Puustinen J, Suortti A-M (2000). Bioremediation of petroleum hydrocarbon-contaminated soil by composting in biopiles. Environmental Pollution 107(2):245-254.
Juhasz AL, Naidu R (2000). Review: Bioremediation of high molecular weight polycyclic aromatic hydrocarbons: a review of the microbial degradation of benzo[*a*]pyrene. International Biodeterioration and Biodegradation 45(2):57-88.
Kanaly R, Harayama S (2000). Biodegradation of high-molecular weight polycyclic aromatic hydrocarbons by bacteria. Journal of Bacteriology 182:2059-2067.
Khajiagbe B, Chijioke - osuji CC, Osazee JO (2014). Heavy metal contents and microbial diversity of waste engine oil polluted soil in some public and commercial centres in Benin City metropolis, Nigeria. The Bioscientist 2(1):41-53.
Kuppusamy S, Thavamani P, Venkateswarlu K, Lee YB, Naidu R, Megharaj M (2017). Review Remediation approaches for polycyclic aromatic hydrocarbons (PAHs) contaminated soils: Technological constraints, emerging trends and future directions. Chemosphere 168:944-968.
Igbiri S, Udowelle NA, Ekhator OC, Asomugha RN, Igweze ZN, Oriskwe OE (2017). Polycyclic Aromatic Hydrocarbons In Edible Mushrooms from Niger Delta, Nigeria: Carcinogenic and Non-Carcinogenic Health Risk Assessment. Asian Pacific Journal of Cancer Prevention: APJCP, 18(2):437.
Ma J, Yang Y, Dai X, Chen Y, Deng H, Zhou H, Guo S, Yan G (2016). Effects of adding bulking agent, inorganic nutrient and microbial inocula on biopile treatment for oil-field drilling waste. Chemosphere 150:17-23.
Malachova K, Lednická D, Novotný C (2003). Genotoxicity Estimation in Soils Contaminated with Polycyclic Aromatic Hydrocarbons after Biodegradation. The Utilization of Bioremediation to Reduce Soil Contamination: Problems and Solutions Pp.211-215.
Nisbet CT, LaGoy PK (1992). Toxic equivalency factors (TEFs) for polycyclic aromatic hydrocarbons (PAHs). Regulatory Toxicology and Pharmacology 16(3):290-300.
Okparanma RN, Ayotamuno JM, Davis DD, Allagoa M (2011). Mycoremediation of polycyclic aromatic hydrocarbons (PAH)-contaminated oil-based drill-cuttings. African Journal of Biotechnology 10:5149-5156.
Paladino G, Arrigoni JP, Satti P, Morelli I, Mora V, Laos F (2016). Bioremediation of heavily hydrocarbon-contaminated drilling wastes by composting. International Journal of Environmental Science and Technology 13:2227-2238.
Phan C-W, Sabaratnam V (2012). Potential uses of spent mushroom substrate and its associated lignocellulosic enzymes. Applied Microbiology and Biotechnology 96:863-873.
Peng Y, Buekens A, Tang M, Lu S (2018). Mechanochemical treatment of fly ash and de novo testing of milled fly ash Environmental Science and Pollution Research 25:19092-19100.
Pies C, Hoffman B, Petrowsky J, Yang Y, Ternes TA, Hofmann T (2008). Characterization and source identification of polycyclic aromatic hydrocarbons (PAHs) in river bank soils. Chemosphere 72:1594-1601.
Shaffer GP, Hester MW, Miller S, Des Rochers DJ, Southern RF, Childers GW, Campo FM (1998). Restored drill cuttings for wetland creation: results of a two-year mesocosm approach to emulate field conditions under varying hydrologic regimes (No. DOE/BC/14849-3). Houston, Texas. Retrieved from https://digital.library.unt.edu/ark:/67531/metadc687884/m1/2/
Shuttleworth KL, Cerniglia E (1995). Environmental aspects of PAH biodegradation. Applied Biochemistry and Biotechnology 54:291-302.
Song H-G (1999). Comparison of pyrene biodegradation by white rot fungi. World Journal of Microbiology and Biotechnology 15:669-672.
Tuomela M, Vikman M, Hatakka A, Itävaara M (2000). Biodegradation of lignin in a compost environment: a review. Bioresource Technology 72(2):169-183.
Venosa AD, Holder EL (2007). Biodegradability of dispersed crude oil at two different temperatures, Marine Pollution Bulletin 54:545-553.
Yunker MB, Macdonald RW, Vingarzan R, Mitchell, RH, Goyette D, Sylvestre S (2002). PAHs in the Fraser River basin: a critical appraisal of PAH ratios as indicators of PAH source and composition. Organic Geochemistry 33:489-515.
Zhang W, Zhang S, Wan C, Dapan W, Youbin Y, Wang X (2008). Source diagnostics of polycyclic aromatic hydrocarbons in urban road runoff, dust, rain and canopy throughfall. Environmental Pollution 153:594-601.

Related Journals: